Bioorganic Chemistry 142 (2024) 106935

Contents lists available at ScienceDirect

Bioorganic Chemistry

journal homepage: www.elsevier.com/locate/bioorg

Exploring the reactivity of bicyclic α-iminophosphonates to access new imidazoline I_2 receptor ligands

Andrea Bagán [a], Sònia Abás [a], Judith Palà-Pujadas [a], Alba Irisarri [b], Christian Griñán-Ferré [b,c], Mercè Pallàs [b], Itziar Muneta-Arrate [d], Carolina Muguruza [d], Luis F. Callado [d,e], Belén Pérez [f], Elies Molins [g], José Á. Morales-García [h], Carmen Escolano [a,*]

[a] Laboratory of Medicinal Chemistry (Associated Unit to CSIC), Department of Pharmacology, Toxicology and Medicinal Chemistry, Faculty of Pharmacy and Food Sciences, and Institute of Biomedicine (IBUB), University of Barcelona, Av. Joan XXIII, 27-31, E-08028 Barcelona, Spain
[b] Pharmacology Section, Toxicology and Medicinal Chemistry, Faculty of Pharmacy and Food Sciences, and Institut de Neurociències, University of Barcelona, Av. Joan XXIII, 27-31. E-08028, Barcelona, Spain
[c] Centro de Investigación Biomédica en Red Enfermedades Neurodegenerativas (CiberNed), National Institute of Health Carlos III, 28029 Madrid, Spain
[d] Department of Pharmacology, University of the Basque Country, UPV/EHU, E-48940 Leioa, Bizkaia, and Centro de Investigación Biomédica en Red de Salud Mental, CIBERSAM, Spain
[e] Biocruces Bizkaia Health Research Institute Bizkaia, Spain
[f] Department of Pharmacology, Therapeutic and Toxicology. Autonomous University of Barcelona, E-08193 Cerdanyola, Spain
[g] Institut de Ciència de Materials de Barcelona (CSIC), Campus UAB, E-08193 Cerdanyola, Spain
[h] Department of Cell Biology. School of Medicine, Complutense University (UCM), 28040 Madrid, Spain

ARTICLE INFO

Keywords:
Imidazoline I_2 receptors
imidazoline I_2 receptor ligands
Neuroprotection
Neuroinflammation
Bicyclic α-aminophosphonate
Bicyclic α-phosphoproline
Alzheimer's disease
Parkinsonism
Caenorhabditis elegans

ABSTRACT

Recent studies pointed out the modulation of imidazoline I_2 receptors (I_2-IR) by selective ligands as a putative strategy to face neurodegenerative diseases. Foregoing the classical 2-imidazoline/imidazole-containing I_2-IR ligands, we report a family of bicyclic α-iminophosphonates endowed with high affinity and selectivity upon I_2-IR and we advanced a representative compound B06 in preclinical phases. In this paper, we describe the synthetic possibilities of bicyclic α-iminophosphonates by exploring its ambivalent reactivity, leading to unprecedented molecules that showed promising activities as I_2-IR ligands in human brain tissues and good BBB permeation capabilities. After *in silico* ADME prediction studies, we assessed the neuroprotective properties of selected compounds and beneficial effect in an *in vitro* model of Alzheimeŕs and Parkinson's disease. Along with their neuroprotective effect, compounds showed a potent anti-inflammatory response when evaluated in a neuroinflammation cellular model. Moreover, this is the first time that the neuroprotective effects of imidazoline I_2-IR ligands in a transgenic Alzheimer's disease *Caenorhabditis elegans* strain are investigated. Using a thrashing assay, we found a significant cognition improvement in this *in vivo* model after treatment with the new bicyclic α-phosphoprolines. Therefore, our results confirmed the need of exploring structurally new I_2-IR ligands and their potential for therapeutic strategies in neurodegeneration.

1. Introduction

Imidazoline I_2 receptors (I_2-IR) are nonadrenergic binding sites that can be found in the central nervous system (CNS) and many other organs such as the heart and the liver [1–3]. The current consensus is that I_2-IR are not a specified molecular identity but heterogenous proteins that are recognized by the radiolabeled ligand [^{3}H]idazoxan and, with much lower affinity, by the [^{3}H]clonidine and the [^{3}H]*p*-aminoclonidine [4,5]. The modulation of I_2-IR by standard ligands evidenced their role in different physiological functions such as analgesia [6], inflammation [7], and human brain disorders [8] encompassing glial tumors [9], depression [10], Alzheimer's disease (AD) [11] and Parkinson's disease (PD) [12,13], amongst others. The chemical structure of I_2-IR ligands [14] is restricted to 2-heterocyclic-2-imidazolines in the standards idazoxan, tracizoline, BU224, 2-BFI and BU99008 or the *N*1-imidazole heterocyclic scaffold in CR4056 (Fig. 1). I_2-IR are emerging as new therapeutic targets, which is endorsed by ongoing clinical trials of CR4056 for the osteoarthritis (phase II) [15] and ^{11}C-BU99008 PET for

* Corresponding author.
E-mail address: cescolano@ub.edu (C. Escolano).

https://doi.org/10.1016/j.bioorg.2023.106935
Received 2 July 2023; Received in revised form 19 October 2023; Accepted 21 October 2023
Available online 24 October 2023

the diagnostics of AD (phase I) [16].

We have contributed to disclosing the pharmacological role of I_2-IR by assessing their modulation with original I_2-IR ligands and by observing *in vivo* physiological responses and modifications of molecular AD-biomarkers in treated murine animal models. We reported the outstanding binding affinity and selectivity for I_2-IR [17] of (2-imidazolin-4-yl)phosphonates [18] synthesized by a microwave assisted multicomponent reaction (Fig. 2A) [19]. The treatment of a murine model of age-related cognitive decline model, the senescence-accelerate mouse prone 8 (SAMP8) with a representative compound, diethyl [(1-(3-chloro-4-fluorobenzyl)-5,5-dimethyl-4-phenyl-4,5-dihydro-1*H*-imidazol-4-yl]phosphonate (named as MCR5) resulted in a cognitive improvement and amelioration of AD hallmarks, including the behavioral [20] and psychological symptoms of dementia [21]. This work was the first experimental evidence that brought forward I_2-IR as a new therapeutic target for neurodegeneration. In addition, MCR5 also improved *in vivo* age-related endothelial dysfunction [22]. We described the potential of [(2-benzofuran-2-yl)-1*H*-imidazole] (named as LSL60101) as a disease-modifying single therapy [23] for the treatment of AD. We also synthesized and pharmacologically characterized a family of congeners embodying the benzofuranyl-2-imidazole skeleton (Fig. 2B) [24]. Moving further with the above-mentioned structures, we described the first I_2-IR ligand that did not feature an imidazoline/imidazole ring. Particularly, we reported a family of bicyclic α-iminophosphonates [25] as a source of high affinity I_2-IR molecules that permitted to carry out a three-dimensional quantitative structure–activity relationship (3D-QSAR). This study revealed key structural parameters that allowed the proposal of a putative pharmacophore for these I_2-IR ligands. We selected the representative compound diethyl (1*RS*,3a*SR*,6a*SR*)-5-(3-chloro-4-fluorophenyl)-4,6-dioxo-1-phenyl-1,3a,4,5,6,6a-hexahydropyrrolo[3,4-*c*]pyrrole-1-phosphonate (named as B06), with excellent activity and selectivity, for the targeted receptors. B06 ameliorated the cognitive decline and improved the behavior of two murine models, SAMP8 [26] and the familial Alzheimer's disease (5xFAD) [27]. Furthermore, B06 showed de-risked *in vitro* ADME-Tox properties and neuroprotective/anti-inflammatory properties as well as neuroprotective effects in an *in vitro* model of PD [28]. Further and more advanced preclinical development studies of B06 in AD and PD brain disorders is underway (Fig. 2C).

Encouraged by the excellent above-mentioned results obtained when we uncovered the novel I_2-IR ligands' chemical structure of I_2-IR ligands, herein we report the synthetic exploitation of the bicyclic α-iminophosphonates by considering the ambivalent properties (C imine- electrophile/C-3a- nucleophile) of the right-inferior quadrant of the molecule leading to the general bicyclic α- phosphoproline structures depicted in Fig. 2C. α-Aminophosphonates, the ubiquitous functional group commonly present in our new compounds, are considered phosphonic analogues of α-aminoesters, which can be applied as an antibiotic, anticancer and antifungal therapies, and are also enzyme inhibitors due to their tetrahedral structure, able to mimic transition states. α-Aminoesters have been used as scaffolds to synthetize peptidomimetic structures and also to study the mode of action of aminoacids in biomedical transformations [29–33]. In this paper we provide a new synthetic strategy to access diversely substituted bicyclic pyrrolidine-2-phosphonates (phosphoprolines, the phosphonic counterpart of proline) [34–36] and evaluate their anti-AD properties.

Diversely substituted (octahydropyrrolo[3,4-*c*]pyrrol-1-yl)phosphonates were synthesized from previously described bicyclic α-iminophosphonates [27] by reduction of the imine group or nucleophilic addition to the C-imine functional group. We assessed the pharmacological profile of selected new compounds in human tissues and their selectivity versus the related target α_2-adrenergic receptor (α_2-AR) by competitive binding assays against the selective I_2-IR radioligand [^{3}H]2-BFI, and competitive studies using the selective radioligand [^{3}H]RX821002 (2-methoxyidazoxan), respectively. We carried out *in vitro* PAMPA-BBB assay for the new molecules and evaluated three selected new compounds in a dopaminergic neurodegeneration cellular model. Furthermore, since most neurodegenerative diseases (AD, PD) are characterized by the presence of an exacerbated and sustained neuroinflammatory process, which is partly responsible for the development of the disease, we completed the study of the *in vitro* biological activity using a cellular neuroinflammation model. Furthermore, since most neurodegenerative diseases (AD, PD) are characterized by the presence of an exacerbated and sustained neuroinflammatory process, which is partly responsible for the development of the disease, we have completed the study of the *in vitro* biological activity using a cellular neuroinflammation model. The positive results motivated us to take the challenge to carry out the first study of the effects after treatment with I_2-IR ligands in the *in vivo* AD model organism *Caenorhabditis elegans* [37]. To this purpose, we used the transgenic strain CL2006 to evaluate the neuronal behavioral phenotype effects of the selected compounds on a thrashing assay. CL2006 expresses human Aβ1-42 under control of a muscle-specific promoter and responds to Aβ1-42 aggregation with progressive adult-onset paralysis. Due to the novelty of the proposal, we included the standard I_2-IR ligand 2-BFI (Fig. 1) endowed with neuroprotective properties [38–40], and three new compounds with optimal affinity upon these receptors.

Finally, exploring further synthetic transformations, tetradecahydrobipyrrolo[3,4-*c*]pyrrole-1,1′-diphosphonates were obtained by self-reaction of ambivalent bicyclic α-iminophosphonates in acid conditions after the nucleophilic attack of the C3a to the imine functional group to other congener.

All new compounds were characterized and described from a stereochemical point of view by X-ray crystallographic analysis as well as

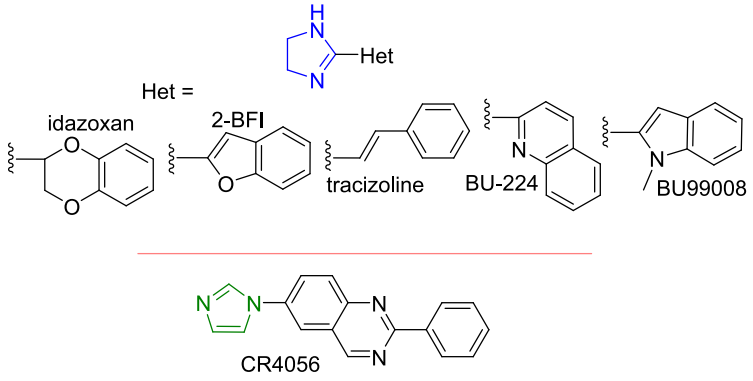

Fig. 1. Structure of the known I_2-IR ligands, imidazoline 2-heterocyclic substituted (idazoxan, 2-BFI, tracizoline and BU224), and clinical candidates (BU99008 and CR4056). The imidazoline nucleus is highlighted in blue and the imidazole nucleus in green. (For interpretation of the references to colour in this figure legend, the reader is referred to the web version of this article.)

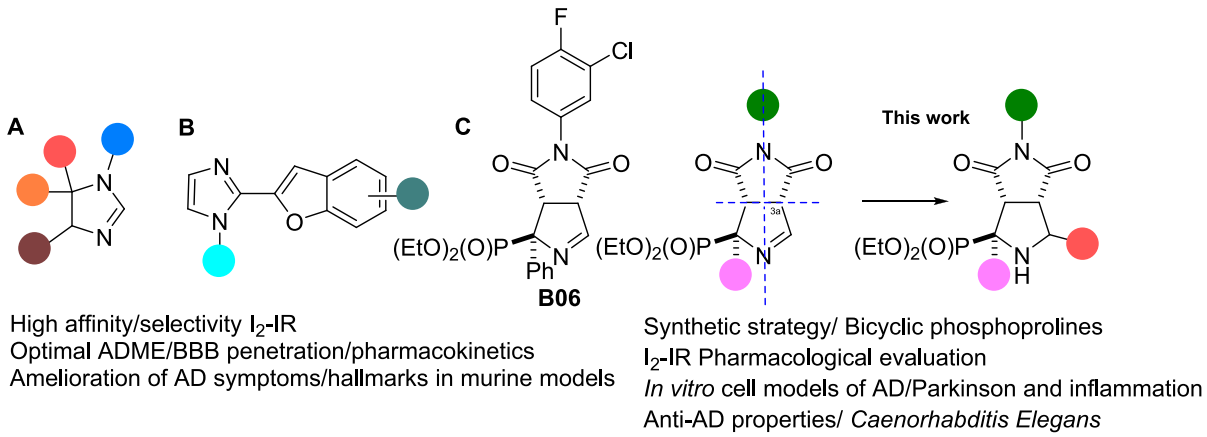

Fig. 2. General structures of the families of I_2-IR ligands reported by our group: A. (2-Imidazolin-4-yl)phosphonates; B. Benzofuranyl-2-imidazoles and C. Chemical structure of B06. Bicyclic α-iminophosphonates and general structure resulting from this work and outlines. Coloured balls indicate a wide-range of substituents.

^{1}H and ^{13}C RMN comparative studies. ADME *in silico* predictions of the new molecules were also included.

2. Results and discussion

2.1. Chemistry

2.1.1. Diastereoselective [3 + 2]cycloaddition reaction

In order to access enough quantities of starting bicycles (Schemes 1 and 2), we undertook their synthesis by following our reported procedure involving a diastereoselective [3 + 2]cycloaddition reaction [27].

2.1.2. Reduction of the imine functional group

The conversion of the diethyl (3,4-dihydro-2*H*-pyrrol-2-yl)phosphonate moiety of bicyclic derivatives to diethyl (pyrrolidine-2-yl) phosphonate required the reduction of the imine functional group. This transformation was already explored though the hydrogenation of compounds **B03**, **B24** and **B02** at atmospheric pressure in order to give access to **B03-red**, **B24-red,** and **B02-red** in 84, 90 and 87 % yield,

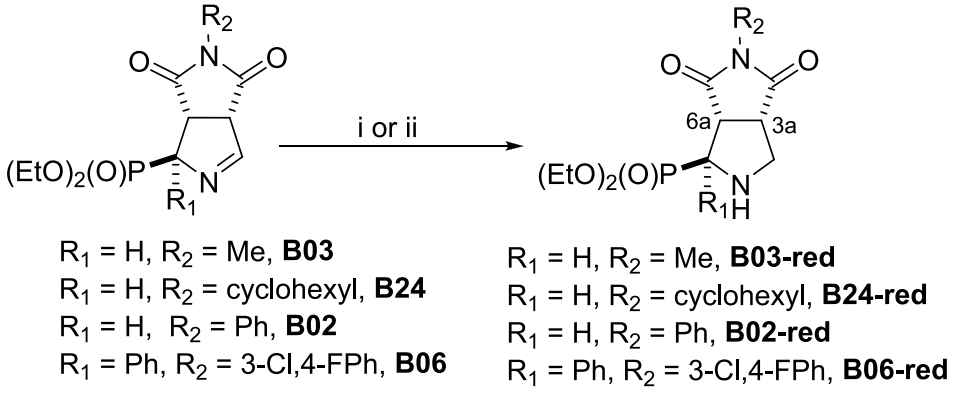

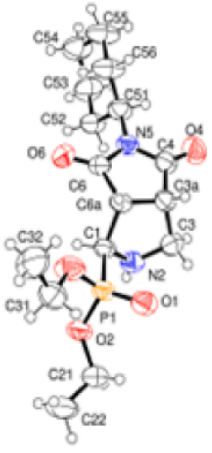

Scheme 1. Reagents and conditions for the reduction of B03, B24, and B02. (i) H_2, Pd/C 5 %, methanol, rt, 24 h, 84 %, B03-red; 90 %, B24-red, and 87 %, B02-red and for B06 (ii) $NaBH_3CN$, acetonitrile, water and acetic acid, rt, 1 h, 84 %, B06-red.HCl. X-Ray crystallographic structure of B24-red.

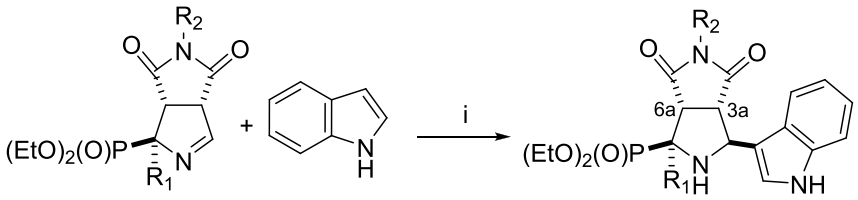

R_1 = H, R_2 = Ph, **B02**
R_1 = R_2 = Ph, **B16**
R_1 = Ph, R_2 = 3-Cl,4-FPh, **B06**
R_1 = Ph, R_2 = 3-ClPh, **B53**

R_1 = H, R_2 = Ph, **BIN01**
R_1 = R_2 = Ph, **BIN02**
R_1 = Ph, R_2 = 3-Cl,4-FPh, **BIN05**
R_1 = Ph, R_2 = 3-ClPh, **BIN06**

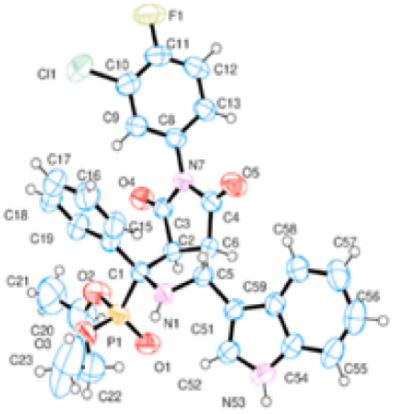

Scheme 2. Aza Friedel Crafts reaction. Reagents and conditions: (i) $AgBF_4$, tetrahydrofurane, r.t., 48 h, 56 %, BIN01; 85 %, BIN02; 64 %, BIN05; and 59 %, BIN06. X-Ray crystallographic structure of BIN05.

respectively [41]. Although the relative configuration of the final products was proposed based on the X-ray analysis of the starting materials and assuming that no new stereocenter was generated [27], here we report the crystal structure of compound **B24-red**, unequivocally confirming a *trans* relationship between the bridgehead hydrogens (H-3a and H-6a) and the hydrogen atom that occupies the α-phosphonate position. The reduction of α-phenyl substituted **B06** was undertaken swiftly with sodium cyanoborohydride for 1 h, followed by treatment with EtOH·HCl leading to the hydrochloride **B06-red** in an 84 % yield (Scheme 1).

By this procedure, α-monosubstituted **B03-red**, **B24-red, B02-red** or α-disubstituted **B06-red** bicyclic pyrrolidine-2-ylphosphonates (bicyclic phosphoprolines) were synthesized confirming the versatility of the starting materials.

2.1.3. *Nucleophilic addition of indole to the imine functional group*

The imine functional group enhances the growth in complexity of the molecule by introducing a new substituent and, in consequence, the generation of a new stereocenter. In this regard, previous work by Prof. J. C. Carretero [42] inspired the experimental conditions used to introduce an indole at the C-3 via an aza Friedel-Crafts reaction. Thus, we performed the reaction by stirring at room temperature during 24 h a mixture of 1 equivalent of **B02**, 1.5 equivalents of silver tetrafluoroborate as a Lewis acid, 2 equivalents of indole, and tetrahydrofuran as the solvent. In these experimental conditions, **BIN01** was isolated in a 43 % yield. Keeping the proportion of the reagents but heating the reaction mixture at 50 °C, the yield of **BIN01** remains similar (45 %). Alternatively, by stirring the mixture at room temperature, re-adding silver tetrafluoroborate and indole, and increasing the reaction time to 48 h, the yield of **BIN01** was 56 %. Having found the best reaction conditions, we considered adding the indole to α-phenyl iminophosphonate bicycles that were non-substituted at the *N*-phenyl ring, **B16**, or are substituted in the *N*-phenyl ring, **B06** (3Cl,4F), and **B53** (3Cl). The final expected products: **BIN02**, **BIN05** and **BIN06**; were isolated in an 85 %, 64 % and 59 % yield, respectively (Scheme 2) [43]. In all cases, only one diastereoisomer was isolated, confirming the exclusive addition of the indole by one face of the bicyclic system.

To unequivocally disclose the relative stereochemistry generated with the introduction of a C-3 new substituent, we prepared a monocrystal of **BIN05** that was studied by X-ray crystallography (Scheme 2). The indole substituent occupied the same face as the phosphonate functional group and the two atoms of hydrogen in the bridgehead positions (H-3a and H-6a). Therefore, the addition of the indole by the *exo* face (convex fashion) of the bicyclic system avoiding steric congestion. To determine if all final compounds depicted in Scheme 2 possess the same relative stereochemistry, we compared the ^{1}H and ^{13}C NMR spectra of unequivocally described **BIN05** with **BIN01**, **BIN02** and **BIN06** (Table 1).

The chemical shift multiplicity and coupling constants of the different protons and carbons were in concordance with the stereochemistry confirmed in **BIN05**. Taking a closer look to the ^{1}H NMR spectra, H6a has coupling constants of 18 Hz (**BIN01**) and 15.0 Hz (**BIN02, BIN05, BIN06**) (H6a-P), 9.5 Hz (all compounds) (H6a-H3a) and 7.0 Hz (**BIN01**) (H6a-H1). In **BIN01**, the H3a appeared with a multiplicity of dd with coupling constants of 9.5 Hz (H3a-H6a) and 8.0 Hz (H3a-H3), while in the α-phenyl substituted compounds it showed a ddd with coupled constants of 9.5 Hz (H3a-H3), 5.5 Hz (H3a-H3), and 1.0 Hz (H3a-P). In the ^{13}C NMR spectra there were additional coupling constants due to the presence of the phosphorous atom in the molecules, such as 165.5 Hz at 57.0 ppm (C1-P) in the α-unsubstituted **BIN01** and 156.5 Hz at 70.4–70.6 ppm in the α-phenyl substituted **BIN02**, **BIN05** and **BIN06**. The C3 appeared as a doublet due to the coupling with the

Table 1
Significant ^{1}H and ^{13}C NMR data, chemical shift, multiplicity and coupling constants (Hz) of **BIN01**, **BIN02**, **BIN05** and **BIN06.**

Comp	H3	H3a	H6a	C1	C3	C3a	C6a	C4	C6
BIN01	4.59	3.68	3.96	57.0	61.4	52.6	48.6	175.1	175.3
	d	dd	ddd	d	d	d	d		
	8.0	9.5, 8.0	18.0, 9.5,7.0	165.5	17.0	7.5	2.0		
BIN02	5.27	3.88	4.47	70.5	58.2	55.9	56.8	172.9	176.2
	m	ddd	dd	d	d	d			
		9.5,5.5,1.0	15.0, 9.5	156.5	15.0	10.0			
BIN05	5.29	3.83	4.44	70.6	58.3	55.8	56.8	172.5	175.9
	d	ddd	dd	d	d	d			
	6.5	9.5, 5.5,1.0	15.0, 9.5	156.5	15.0	10.0			
BIN06	5.29	3.85	4.45	70.4	58.2	55.7	56.7	172.4	175.8
	d	ddd	dd	d	d	d			
	5.5	9.5, 5.5,1.0	15.0, 9.5	156.5	15.0	10.0			

m = multiplet, ddd = doublet of doublet of doublets, dd = doublet of doublets, d = doublet.

phosphorous atom with a value of 17 Hz for **BIN01** and 15.0 Hz for the α-phenyl substituted derivatives. The interaction of the C3a-P led to coupling constants of 7.5 Hz (**BIN01**) and 10.0 Hz (**BIN02, BIN05, BIN06**) (Fig. 3).

To further explore the reactivity of the prepared compound, the opening of the imide containing ring was carried out. To this end, the treatment of **BIN02** with sodium hydroxide at room temperature during 2.5 h led to an unexpected monocyclic compound, lacking the phosphonate ester functional group and with an 80 % yield. The analysis of the ^{1}H and ^{13}C NMR spectra and the X-ray crystallography led to the unequivocal description of the new structure **PIP-BIN02** (Scheme 3).

The formation of **PIP-BIN02** could be accounted by considering the attack of the hydroxide anion to the C6, which underwent the opening of the imide function and the generation of an intermediate. The latter decarboxylated and extruded the phosphonate ester to lead the trisubstituted 1-pyrroline **PIP-BIN02** (Scheme 4).

In this scenario, the phosphonate functional group works was an auxiliary group that allowed the initial diastereoselective [3 + 2] cyclocondensation to occur (by increasing the acidity of the α-proton). Furthermore, this phosphonate functional group orientated the diastereoselective entry of the indole substituent and, finally, it was displaced in the basic treatment to afford **PIP-BIN02.**

2.1.4. The bridgehead position of bicyclic α-iminophosphonates as a nucleophile

The addition of nucleophiles to the carbon of the imine function increased the structural complexity of the new molecules (section 2.1.3.), which led us to consider the ambivalent nature of the starting bicyclic α-iminophosphonates. Thus, in the same molecule there was a nucleophilic position, such as C3a (α-carbonyl of an amide and the α-imine position), and an electrophilic position C3 (carbon of the imine). The amphiphilic characteristic in the two different positions of the same molecule was also observed in the unique carbon atom of the isocyanide group of the starting materials, PhosMIC or α-PhPhosMIC, employed in the [3 + 2]cycloaddition reaction (section 2.1.1.) that could react either with nucleophiles or electrophiles [46].

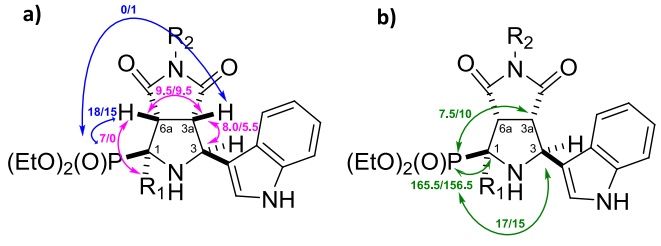

Fig. 3. Representative coupling constants: a) ^{1}H–^{1}H (pink), ^{1}H-P (blue) and, b) ^{13}C-P (green) for BIN01/BIN02, BIN05, BIN06. (For interpretation of the references to colour in this figure legend, the reader is referred to the web version of this article.)

Therefore, we took the challenge of accessing "dimeric diphosphonate bicycles" depicted in Scheme 5. To this end, we treated **B02** with 3 equivalents of trimethysilyl chloride (TMSCl) in dichloromethane at room temperature during 48 h. The crude mixture was purified leading to the identification of two compounds with the same molecular mass (diastereoisomers) in a 1:2 proportion (GC/MS determination) and a 59 % yield, which named **BxB03/BxB04** (Table 2, entry 1)**.** Increasing TMSCl to 6 equivalents led to a mixture of 1:1.6 ratio of **BxB03/BxB04** in a 45 % yield (Table 2, entry 2). The use of microwave irradiation at 80 °C during 30 min gave a 68 % yield of a 1:1.7 **BxB03/BxB04** mixture (Table 2, entry 3) and 16 % of starting material. Conducting the reaction by using the *N*-methyl derivative **B03** under conditions of entry 2, led to a 64 % yield of a 1:2.2 mixture of **BxB01/BxB02** (Table 2, entry 6). Analogously to conditions in entry 3, **B03** rendered a 58 % mixture 1:1.4 of **BxB01/BxB02** (Table 2, entry 7) and 3 % of starting material. Inspired by the work of M. Noguchi [45], we used the milder acid pyridinium *p*-toluensulphonate (PPTS), which triggered the dimerization of **B02** after treatment with 1.5 equivalents at reflux temperature during 15 h providing a 57 % yield of a 1:0.8 mixture of **BxB03/BxB04** (Table 2, entry 4). The microwave irradiation at 80 °C for 40 min slightly decreased the reaction yield (46 %) but it maintained the proportion of the final products (Table 2, entry 5). The conditions depicted in entry 4 led to a 1:0.9 mixture of **BxB01/BxB02** in a 57 % yield when **B03** was used as starting material (Table 2, entry 8). Similarly, to the results described in entry 5 when applying to **B03**, an equitable mixture of **BxB01/BxB02**, was isolated in a 43 % yield (Table 2, entry 9). The use of the two different acids (TMSCl and PPTS) led to similar results with both **B02** and **B03** as starting bicycles with a ratio of final dimers ~ 1:1.4–2 with TMSCl and 1:0.8–1 PPTS. Therefore, the substituent in the nitrogen atom, *N*-Me (**B02**) or *N*-Ph (**B03**), does not affect the course of the "dimerization" reaction.

Next, we examined the influence that an α-additional substituent could play in the results of the reaction results compared to the presence of a hydrogen atom. To this end, compound **B16**, that embodies a α-phenyl substituent, was heated at 80 °C with 6 equivalents of TMSCl in a microwave oven for 30 min. The expected dimers **BxB05/BxB06** were isolated in a 1:1.5 ratio and a 68 % yield, along with a 15 % of **B16**. Consequently, the studied reaction took place in a similar fashion, regardless the presence or not of substituents in the α-position.

In the dimerization reaction, a new bond, a quaternary stereocenter in the bridged position (C3a) and a stereocenter in the carbon atom contiguous to the nitrogen (C3′) were generated. The configurations of the C1, C6a and C3a (and C1′, C6a' and C3a') were fixed, due to the stereochemical result of the diastereoselective [3 + 2]cycloaddition reaction of the *N*-methyl, or *N*-phenylmaleimide, with PhosMIC of α-PhPhosMic (Scheme 5). Considering that the starting **B02**, **B03** and **B16** were racemic mixtures, the dimerization reaction could proceed either between the same enantiomer or between different enantiomers. Therefore, although only two pairs of enantiomers were isolated, eight possible stereoisomers (four pairs of enantiomers) should be considered

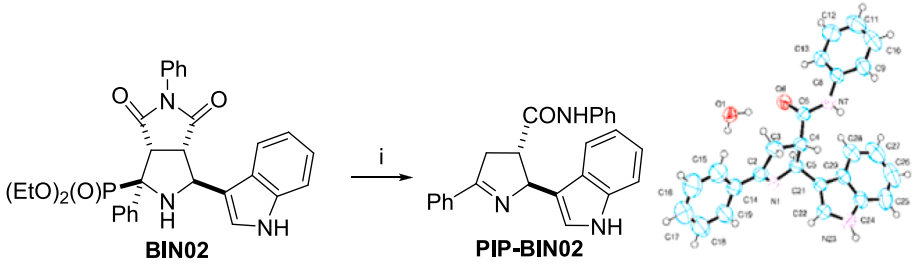

Scheme 3. Reagents and conditions for the synthesis of PIP-BIN02 (i) NaOH 0.05 M, tetrahydrofuran: water (2:1), r.t., 2.5 h, 80 % yield. X-Ray crystallographic structure of PIP-BIN02.

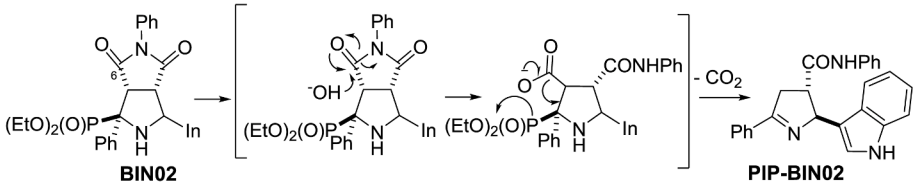

Scheme 4. Putative mechanism for the formation of PIP-BIN02. In = indole.

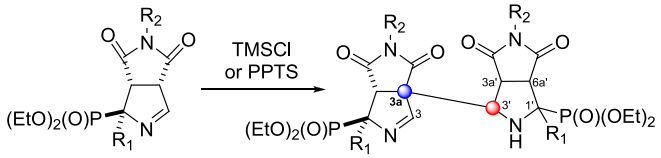

Scheme 5. Reaction of B02, B03 and B16 with TMSCl or PPTS and general structure of the dimers BxB03/BxB04, BxB01/BxB02 and BxB05/BxB06. New quaternary stereocenter highlighted in blue, and new stereocenter highlighted in red.

Table 2
Reaction conditions and yield (ratio) to access dimeric (**BxB01/BxB02**, **BxB03/BxB04**).

Entry	Starting material Reaction conditions	Yield (%)
	B02	**BxB03/BxB04**
1	TMSCl 3 eq, r.t.., CH_2Cl_2, 48 h	59 (1:2)
2	TMSCl, 6 eq, r.t. CH_2Cl_2, 48 h	45 (1:1.6)
3	TMSCl, 6 eq, MW, 80 °C, 30 min	68 (1:1.7)
4	PPTS, 1.5 eq, Δ, MeOH, 15 h	57 (1:0.8)
5	PPTS, 1.5 eq, MW, MeOH, 80 °C, 40 min	46 (1:0.8)
	B03	**BxB01/BxB02**
6	TMSCl 6 eq, r.t.., CH_2Cl_2, 48 h	64 (1:2.2)
7	TMSCl, 6 eq, MW, 80 °C, 30 min	58 (1:1.4)
8	PPTS, 1.5 eq, Δ, MeOH, 15 h	57 (1:0.9)
9	PPTS, 1.5 eq, MW, MeOH, 80 °C, 40 min	43 (1:1)

TMSCl: trimethylsilyl chloride; PPTS: pyridinium p-toluensulphonate; MW: irradiation in a microwave oven.

depending on the face (*exo/endo*) where the reaction took place (Scheme 5).

In general, the addition of nucleophiles to bicyclic systems is more favored through the *exo* face. To confirm this hypothesis, the stereochemistry of **BxB05/BxB06** was indisputably determined by X-ray crystallography analysis (Fig. 4).

Compound **BxB05** results from the *exo* addition of **B16** to the same enantiomer and compound **BxB06** from the *exo* addition to the convex face to the other enantiomer of **B16**.

Aiming to determine the relative stereochemistry in the three pairs of diastereoisomers, we compared the ^{1}H and ^{13}C NMR spectra of **BxB03/BxB04** and **BxB01/BxB02** with the relative configuration confirmed for **BxB05/BxB06** (Tables 3 and 4).

The chemical shift multiplicity and coupling constants of the different protons and carbons were in concordance with the stereochemistry assigned to the pair of compounds **BxB05/BxB06**. Specifically, the difference in the shield between de protons and carbons at the same position was preserved within the three pairs of dimeric compounds (Scheme 5). Thus, the *exo* addition of **B02** to its enantiomer led to **BxB03** and, in the case of **B03**, it led to **BxB01**. The *exo* self-addition of **B02** and **B03** rendered **BxB04** and **BxB02**, respectively.

In detail, in compounds **BxB01-BxB04**, the H1 hydrogen displayed a coupling constant with the phosphorous atom of ~ 22 Hz, and two minors with the H6a and H3 (2.5–4.0 Hz). The bridged H6a' in **BxB01, BxB03** and **BxB04** showed a peak with a multiplicity of ddd due to the coupling constants 17.5–18.0 (H6a'-P), 9.0–10.0 (H6a'-H3a') and 7.0–8.0 Hz (H6a'-H1′).

It is noteworthy that in the ^{13}C spectra C1/C1′ and C3/C3′ were doublets due to the presence of the phosphorous atom with significant coupling constants of C1 (159.5–161.5 Hz)/C1′ (168.0–175-0 Hz) and C3 (13.0–14.0 Hz)/C3′ (14.0–16.5 Hz), respectively. The difference between the C3a within the two members of each pair is conserved (3.5–3.8 ppm) (Fig. 5).

2.2. *In silico prediction of physicochemical and ADME pharmacokinetic properties of new compounds*

With the goal of describing the potential of the new compounds as drug candidates (Scheme 1, 2 and 5), the favorable drug-likeness features were predicted by the validated medchem program molinspiration software [44]. Molinspiration was used to calculate molecular descriptor properties of Lipinski's rule for the new compounds, i.e., molecular weight, number of H-bond donors & acceptors, topological polar surface area (TPSA), log P, and number of rotable bonds (nRotB). The Lipinski rule states that the permeation of an orally administered compound is more likely to be absorbed better if the properties of the molecule are the following: molecular weight < 500, log P < 5, number of hydrogen bond acceptors < 10, and number of hydrogen bond donors < 5. The expansion of Lipinski's rules considers several rotatable bonds < 10 and polar surface area ≤ 140 Å. Compounds depicted in Scheme 1

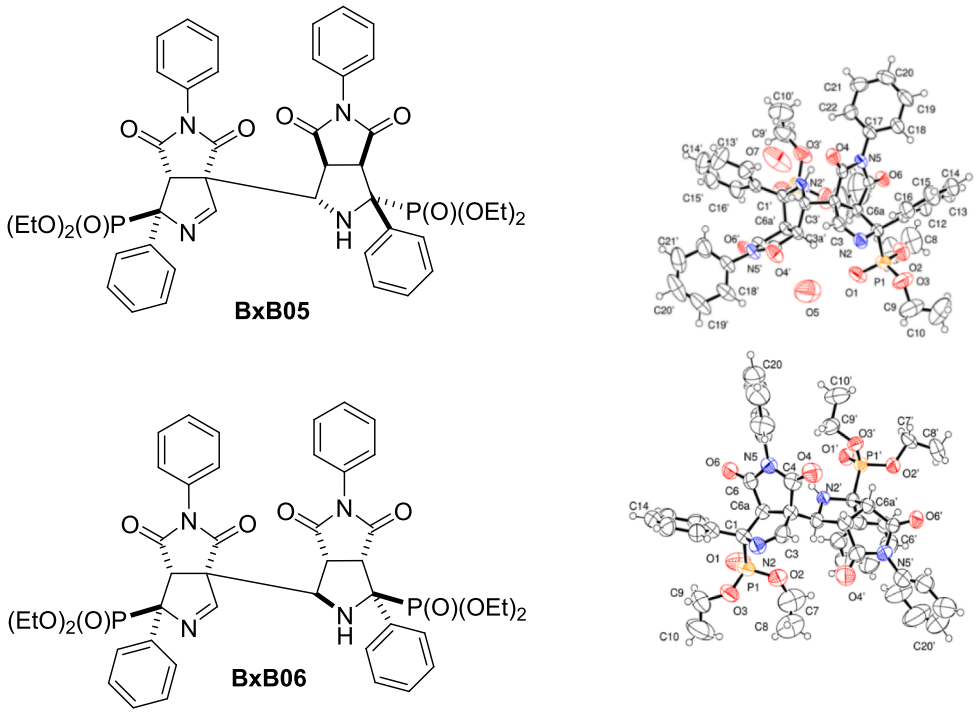

Fig. 4. Chemical structure of BxB05 and BxB06 and their X-ray structures.

Table 3
Significant ^{1}H data of **BxB03/ BxB04, BxB01/ BxB02** and **BxB05/ BxB06.**

Comp.	H1	H3	H6a	H1′	H3′	H3a’	H6a’
BxB01	4.64 dt 22.5, 3.5	7.69 m	3.91 dd 18.5, 4.0	3.46 m	4.33 m	3.97 dd 9.0, 7.0	3.61 ddd 17.5, 9.0, 8.0
BxB02	4.72 ddd 22.0, 3.5, 2.5	7.92 dd 4.5, 2.5	4.02 dd 18.0, 3.5	3.40 ddd 8.0, 5.0, 3.5	4.17–4.33 c.s.	3.54–3.67 c.s.	3.54–3.67 c.s.
BxB03	4.82 ddd 22.5, 4.0, 3.0	7.81 dd 4.0, 3.0	4.10–4.41 c.s.	3.69 m	4.62 t 6.5	4.10–4.41 c.s.	3.86 ddd 18.5, 9.5, 7.5
BxB04	4.89 dt 22.0, 3.0	8.04 dd 4.5, 3.0	4.14 m	3.62 m	3.92 dd 7.0, 5.0	4.57 dd 9.5, 7.5	3.81 ddd 18.0, 10.0, 8.0
BxB05	–	8.16 d 3.5	4.25–4.43 c.s.	–	5.28 m	4.25–4.43 c.s.	4.25–4.43 c.s.
BxB06	–	8.32 d 4.0	4.30–4.43 c.s.	–	4.50 t 5.5	4.70 dd 9.5, 5.0	4.30–4.43 c.s.

m = multiplet, t = triplet, ddd = doublet of doublet of doublets, dd = doublet of doublets, dt = doblet of triplets, c.s = complex signal.

obeyed Lipinski’s rule, and therefore showed good bioavailability. The molecular weights of **BIN02**, **BIN05** and **BIN06** were over 9 %, 19 % and 15 % respectively, lying within the recommended limit for a good bioavailability. The log P of **BIN05** and **BIN06**, were 5.12 and 5.0 respectively, slightly over the < 5 desired value, therefore, good permeability across the cell membrane was expected. **PIP-BIN02** was in full compliance with Lipinski’s rules. Dimers depicted in Scheme 5 were discarded for further biological assays due to their high molecular weight (852.82 for **BxB05** and **BxB06**) and their high number of bond acceptors (14), involving possible insufficient oral drug-likeness characteristics (see supporting information). The pharmacokinetics of the new compounds were predicted using Swiss ADME web-based tool [47]. All compounds showed values classified as very soluble (ESOL and Ali classes) and soluble (Silicos), and exhibited optimal high gastrointestinal absorption, which is a requirement for oral drugs. The prepared molecules were not predicted to be substrates of the cytochromes (CYP1A2, CYP2C19, CYP2C9, CYP2D6 and CYP3A4). No PAINS alerts were showned, and the general predicted parameters matched with a good drug likeness. The results of ADME prediction are detailed in supporting information.

2.3. *Radioligand I_2-IR binding assays*

The pharmacological profile of seven representative compounds with general structures in Schemes 1-3, selected based on comparison with previous reported structures [27], were evaluated by competitive binding studies against the selective I_2-IR radioligand [^{3}H]2-BFI and the selective α_2-AR radioligand [^{3}H]RX821002. The studies were performed in membranes from *post-mortem* human frontal cortex, a brain area that shows an important density of I_2-IR and α_2-AR [48]. Idazoxan, a compound with well-established affinity for I_2-IR ($pK_i = 7.41 \pm 0.63$) and α_2-AR ($pK_i = 8.35 \pm 0.16$), was used for reference [49]. The inhibition

Table 4
Significant ^{13}C NMR data of **BxB03/ BxB04, BxB01/ BxB02** and **BxB05/ BxB06.**

Comp.	C1	C3	C3a	C6a	C1′	C3′	C3a'	C6a'
BxB01	73.3 d 160.0	164.8 d 13.5	74.7	45.2	56.5 d 174.5	61.5 d 15.5	47.9 d 7.5	47.3
BxB02	74.1 d 160.5	164.4 d 13.5	71.1	47.4 d 9.5	56.2 d 174.0	63.2 d 16.0	47.3 d 8.0	47.5
BxB03	73.8 d 159.5	164.8 d 14.0	74.7	48.1 d 7.0	57.0 d 175.0	62.5 d 14.5	45.3	47.5
BxB04	74.7 d 160.0	164.4 d 13.0	70.9	47.5	56.6 d 173.5	63.8 d 16.5	47.4	46.8
BxB05	85.5 d 161.5	164.4 d 14.0	76.0	51.6	67.0 d 172.0	60.6 d 14.0	49.1 d 9.5	53.8
BxB06	86.6 d 160.5	164.1 d 13.5	72.5	53.9	69.0 d 168.0	61.7 d 15.0	49.5 d 10.5	53.3 d 2.5

d = doublet.

constant (K_i) for each compound was obtained and was expressed as the corresponding pK_i. The selectivity for these two receptors was expressed by the I_2/α_2 index, calculated as the antilogarithm of the ratio between pK_i values for I_2-IR and pK_i values for α_2-AR. Competitive experiments against [^{3}H]2-BFI were biphasic for some of the compounds (Table 5).

Basing ourselves results, we compared the pK_i I_2 affinity displayed by **B24** [27] of 5.74 with its reduced analogous **B24-red**, which depicted a negligible affinity upon these receptors (pK_i = 3.32). As previously reported; **B06**, the *N*-3Cl,4F-phenyl and the α-phenylsubstituted analogue fitted significantly better into a two-site binding model, with a high pK_i I_2 8.61 (K_{iH} = 2.45 nM) and a low pK_i I_2 4.29 (K_{iL} = 51.2 μM), with the high-affinity site accounting for a calculated 37 % of the specific binding of the [^{3}H]2-BFI at 2 nM concentration. Its reduced congener **B06-red** showed an outstanding value fitted into two sites with a pK_{iH} of 9.81 and a 50 % occupancy, but a loss of selectivity versus α_2-AR. Therefore, the reduction of the imine functional group did not represent an improvement in the affinity values of the two structures considered. Next, we undertook the pharmacological evaluation of the compounds resulting from the addition of an indole to the C-imine. **BIN01** presented an I_2-IR affinity of pK_i = 7.46, in a similar value range to its partner **B02** (pK_i = 7.73). Neither compound showed selectivity upon α_2-AR. It was worth noting that when comparing non α_2-AR selective **B16** (pK_i = 10.28) with **BIN02**, a decrease in the I_2-IR affinity occurred (7.31), which was still in the range of non-selective idazoxan (pK_i = 7.41), but exhibiting a remarkable selectivity index (5012). The affinity of **BIN05** fitted into a two-fold curve with values within the same range (pK_{iH} 8.18 and pK_{iL} 3.56) of the affinity value for **B06**, but with a lower occupancy of the high-affine site (21 % *vs* 37 % for **B06**) and a lack of selectivity upon α_2-AR. **B53** lacked I_2-IR activity and its 3-indol substituted partner **BIN06** showed pK_{iH} = 7.77 activity but with only a 17 % of high-affinity site-occupancy. Therefore, the introduction of an indol substituent to position 3 of the bicyclic system did not have beneficial outcomes in the affinity values.

Finally, the trisubstituted pyrrolidine **PIP-BIN02** did not reveal interesting biological properties as I_2-IR ligand.

2.4. BBB permeation assay

Considering that the I_2-IR are in the CNS, ease to cross the BBB is an essential requirement for I_2-IR ligands in development with potential therapeutic applications in the neuroprotective field. Therefore, the *in vitro* permeability (Pe) of representative compounds from the novel bicyclic families was determined by PAMPA-BBB permeability assay (Table 6).

Seeing the limits stablished by Di et al. for BBB permeation [50], the compounds **B24- red**, **B06-red**, **BIN02** and **BIN06** were well above the threshold established for high BBB permeation ($P_e > 5.198 \times 10^{-6}$ cm s^{-1}). Compounds **BIN01**, **BIN05** and **PIP-BIN02** were predicted to have an uncertain BBB permeation (CNS +/-): 5.198 > P_e (10^{-6} cm s^{-1}) > 2.054 but they were considered suitable to undergo further *in vitro* and *in vivo* studies to gain more in-depth insights about the pharmacological profile of the new family of I_2-IR ligands.

2.5. Effects of BIN02, BIN05, and B06-red on preclinical models of neurodegeneration in vitro

2.5.1. Neuroprotective role on Alzheimeŕs and Parkinsońs cellular models

Neurons and glial cells (astrocytes and microglia) cultivated *in vitro* in static devices, such as *trans*-well systems, are useful tools for basic linear kinetic studies during drug discovery. The HT-22 mouse hippocampal neuronal cell line is currently recognized as a valuable experimental model for the study of glutamate-induced neurotoxicity associated with AD [51]. Since human neuronal dopaminergic cell line SH-SY5Y shares many characteristics with substantia nigra neurons, it has been established as an appropriate system for simulating the properties of dopaminergic neurons *in vitro* [52]. To assess the possible cytotoxic effect of the compounds, *per se*, we exposed cells to various concentrations of these compounds, ranging from 200 nM to 20 μM. None of the concentrations applied had harmful effects on the cells (Fig. 6).

We then assessed whether the compounds were able to prevent neuronal death caused by exposure to cytotoxic agents, glutamate for HT-22 hippocampal cells, and 6-OHDA for SH-SY5Y dopaminergic neurons (Fig. 7A). Two well-known I_2-IR ligands, idazoxan and 2-BFI (Fig. 1), were considered standard treatments for reference purposes [53]. A cytotoxicity analysis and the effective dose of idazoxan and 2-BFI were previously reported [27]. Qualitatively, our findings reveal that these compounds showed a potent neuroprotective effect in both neuronal *in vitro* models, being able to highly prevent toxin-induced neuronal death.

2.5.2. In vitro evaluation of the anti-inflammatory effect

The extensive and protracted neuroinflammatory process that the CNS experiences as a result of the disease is one of the key causes of

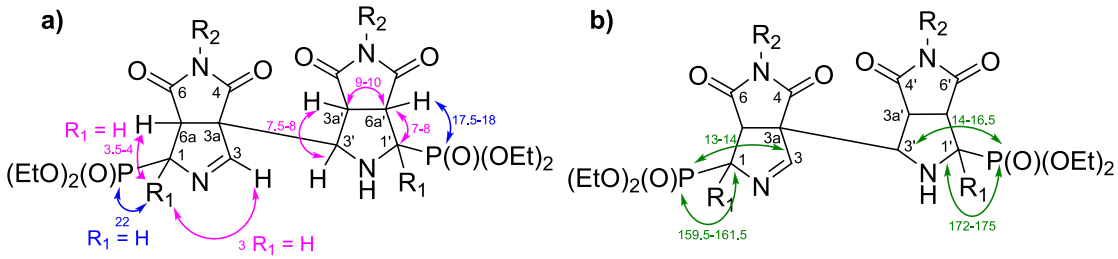

Fig. 5. Representative coupling constants: a) ^{1}H–^{1}H (pink), ^{1}H-P (blue), and b) ^{13}C-P (green) for BxB03/ BxB04, BxB01/ BxB02 and BxB05/ BxB06. (For interpretation of the references to colour in this figure legend, the reader is referred to the web version of this article.)

Table 5
I_2-IR and α_2-AR Binding Affinities (p*Ki*) of compound idazoxan, previously reported **B24**, **B06**, **B02**, **B16**, **B53** and new compounds **B24-red**, **B06-red**, **BIN01**, **BIN02**, **BIN05**, **BIN06** and **PIP-BIN02**.

Compound	[a] [^{3}H] 2-BFI I_2 pK_i (one site) [b] [^{3}H] -2-BFI I_2 pK_i (two sites: pK_{iH}/K_{iL}) High affinity site %	[^{3}H] -RX821002 α_2 pK_i	Selectivity I_2/ α_2
Idazoxan	7.41 ± 0.63	8.35 ± 0.16	
[c]**B24**	5.74 ± 0.51	5.02 ± 0.58	–
B24-red	3.32 ± 0.67	5.38 ± 0.33	–
[c]**B06**	8.56 ± 0.32 8.61 ± 0.28/4.29 ± 0.20 37 ± 4	6.27 ± 0.56	195
B06-red	6.88 ± 0.29 9.81 ± 0.21/<3 50 ± 4	6.66 ± 0.49	1.7
[c]**B02**	7.73 ± 0.19	8.49 ± 0.36	–
BIN01	7.46 ± 0.41	7.87 ± 0.57	–
[c]**B16**	10.28 ± 0.37	10.38 ± 0.22	–
BIN02	7.31 ± 0.39	3.61 ± 0.32	5012
BIN05	3.89 ± 0.19 8.18 ± 0.43/3.56 ± 0.22 21 ± 3	5.51 ± 0.24	–
[c]**B53**	<3	–	
BIN06	5.89 ± 0.30 7.77 ± 0.36/<3 17 ± 2	6.19 ± 0.26	–
PIP-BIN02	3.59 ± 0.26 8.05 ± 0.29/<3 9 ± 2	6.62 ± 0.22	–

[a] Selectivity I_2-IR/α_2-AR expressed as the antilog (pK_i I_2-IR − pK_i α_2-AR). [b] The best fit of the data for most of the compounds was a two-site binding model with high pK_i (pK_{iH}) and low pK_i (pK_{iL}) affinities for both binding sites, respectively. [c] Values published by our group [27].

Table 6
Permeability results (Pe 10^{-6} cm s^{-1}) from the PAMPA-BBB assay for newly reported compounds and their prediction of BBB permeation.

Compound	[a] P_e 10^{-6} cm s^{-1}	[b] Prediction
B24-red	7.1 ± 0.4	CNS+
B06-red	10.2 ± 0.4	CNS+
BIN01	3.1 ± 0.1	CNS+/-
BIN02	8.8 ± 0.4	CNS+
BIN05	5.0 ± 0.2	CNS+/-
BIN06	9.4 ± 0.9	CNS+
PIP-BIN02	4.9 ± 0.3	CNS+/-

[a] PBS/EtOH (70:30) was used as solvent. Values are expressed as mean ± SD of at least three independent experiments.
[b] The *in vitro* permeability (Pe) of fourteen commercial drugs through lipid extract of porcine brain membrane together with the test compounds were determined (for the commercial drug values see Table in the supporting information).

neurodegenerative diseases progression. Therefore, determining whether the compounds could mitigate inflammation was our next goal. A neurotoxic effect induced by glutamate in HT-22 hippocampal neurons and by 6-OHDA in dopaminergic neurons typically causes strong inflammatory activity, in addition to cytotoxicity. Thus, we next investigated the possible anti-inflammatory effects of the compounds by examining the nitrite generation in the cultures exposed to the neurotoxin (Fig. 7B). The treatment with **BIN02**, **BIN05**, and **B06-red** considerably reversed the increase in nitrite generation evoked by the toxins' treatment, supporting the findings from the cell viability assays and pointing to a clear anti-inflammatory effect of the compounds. Notably, all the studied compounds outperformed other I_2-IR ligands, idazoxan and 2-BFI, in terms of its ability to reduce inflammation.

Since the main regulators of the inflammatory response in nervous tissue are glial cells, we next evaluated the role of the compounds in an *in vitro* neuroinflammation model. Interestingly, I_2-IR were found throughout the brain, mainly in glial cells [51], suggesting that this receptor is crucial in neuroinflammation. Therefore, we conducted studies in several cell-based assays that partially imitate the neuroinflammatory process in AD and PD in order to better assess the role of compounds in inflammatory reactions. For this purpose, we used two established glial lines widely used as a cellular model of neuroinflammation, the murine-derived BV2 (microglia) and C6 (astroglia) cells. To enhance this research, we also used primary cultures of mouse cortex-isolated glial cells. In response to a pro-inflammatory agent, such as a LPS, cells released nitrite into the culture medium (Fig. 8). Then, production of nitrites was used to assess the possible anti-inflammatory action of the indicated compounds. Results indicate that **BIN02**, **BIN05** and **B06-red** exhibit a potent anti-inflammatory effect on all glial cultures evaluated in comparison with LPS-treated cultures. Interestingly, cultures treated with these compounds showed lower amount of nitrites when compared to the I_2-IR standard ligands idazoxan and 2-BFI.

2.6. *In vivo efficacy of **2-BFI, B06-red, BIN02, BIN05** on transgenic AD C. Elegans model*

The pharmacological impact of the well-stablished I_2-IR ligand 2-BFI and the selected **B06-red**, **BIN02**, and **BIN05** was evaluated by counting the number of thrashes in CL2006 *C. elegans* strain. Interestingly, all treatments showed a higher number of thrashes in recovery to the vehicle group. In the case of 2-BFI and **BIN05** groups, the increase in the number of thrashes was not statistically significant. On the other, both treatments, **BIN02** and **B06-red**, showed higher number of thrashes, being at least 2-fold more compared to the CL2006 Control group (Fig. 9). Thus, to our knowledge this is the first time, we showed cognitive improvement in *C. elegans* after I_2-IR ligands treatment, suggesting the participation of I_2-IR in the pathogenesis of the cognitive deficits presented in AD.

3. Conclusions

As one of the leading causes of disability worldwide, neurodegenerative disorders have enormous medical, social, and economic implications. Different mechanisms have been involved in the pathogenesis of neurodegenerative diseases, such as oxidative stress, protein aggregation, mitochondrial dysfunction, or excitotoxicity. However, one of the most important events affecting both AD and PD is undoubtedly neuroinflammation. Currently, many efforts are being made towards the development of new treatments that protect neurons and mitigate glial activity, reducing the production of proinflammatory agents, which in turn increases neuronal survival. In this context and supported by previous successful experiences in the exploration of structurally new imidazoline I_2-IR ligands, we have proposed I_2-IR as promising therapeutic target to face neurodegenerative diseases. Here, we examine the synthetic possibilities of bicyclic α-iminophosphonates considering the characteristics of the imine group and the carbon C3a, accessing unprecedented structures that were unequivocally described from the stereochemical point of view and characterized by its affinity/selectivity upon I_2-IR in human brain tissues. We selected three representative compounds, **BIN02**, **BIN05** and **B06-red,** and we demonstrate how I_2-IR ligands, are able to protect neurons from cytotoxic damage in two well-known preclinical models of AD and PD. In addition, these compounds markedly reduce the proinflammatory activity resulting from glial cell activation. Note that, we are reporting the first *in vivo* proof-of-concept of the treatment of *C. elegans* with I_2-IR ligands. Our representative compounds rescue the neurodegenerative condition presented by CL2006 strain at the behavioural phenotype level. Consequently, these results may constitute the basis for considering I_2-IR as anti-AD/PD targets and I_2-IR ligands as future therapeutic hits against these neurodegenerative diseases.

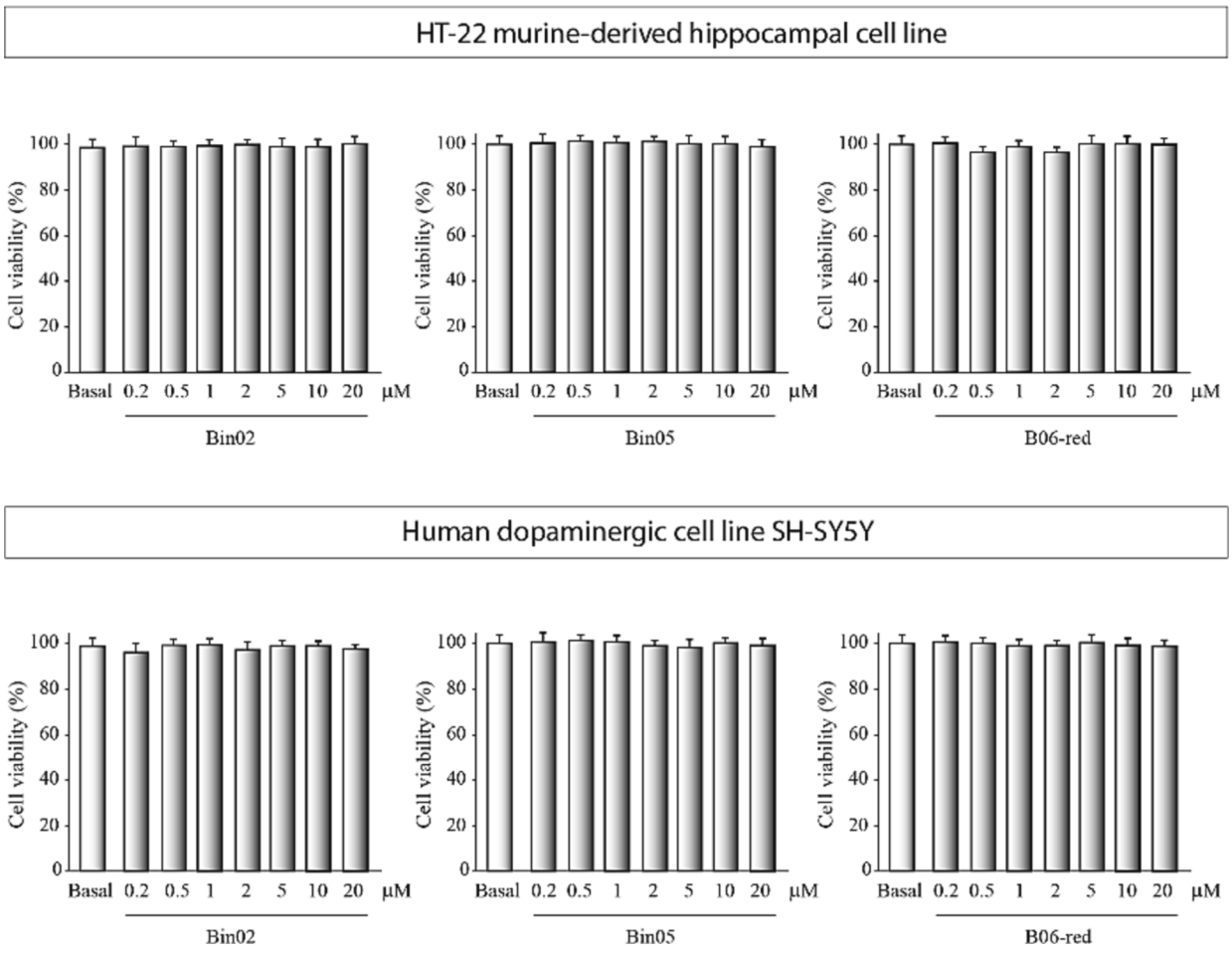

Fig. 6. *In vitro* I_2-IR ligands cytotoxicity analysis. Hippocampal murine-derived HT-22 and SH-SY5Y human dopaminergic cell lines were exposed for 24 h to increasing concentrations of the indicated compounds. A 3-(4,5-dimethylthiazol-2-yl)-5-(3-carboxymethoxyphenyl)-2-(4-sulfophenyl)-2*H*-tetrazolium (MTT) test was used to evaluate I_2-IR ligands' cytotoxic potential. Values are the mean ± SD from triplicate determinations repeated at least three times. After confirming the significance of the results with an analysis of variance, a significance level of $p < 0.05$ was applied to the post hoc statistical analyses (Tukey test).

4. Experimental section

4.1. Chemistry

Reagents, solvents and starting products were acquired from commercial sources. The organic layers were dried over $MgSO_4$. The term "concentration" refers to the vacuum evaporation using a Büchi rotavapor. When indicated, the reaction products were purified by "flash" chromatography on silica gel (35–70 μm) with the indicated solvent system. IR spectra were performed in a Spectrum Two FT-IR Spectrometer, and only noteworthy IR absorptions (cm^{-1}) are listed. NMR spectra were recorded in $CDCl_3$ and DMSO-d_6 at 400 MHz (^1H) and 100.6 MHz (^{13}C), and chemical shifts are reported in δ values downfield from TMS or relative to residual chloroform (7.26 ppm, 77.0 ppm) and DMSO-d_6 (2.50 ppm, 39.5 ppm) as an internal standard. Data are reported in the following manner: chemical shift, multiplicity, coupling constant (*J*) in hertz (Hz) and integrated intensity. Multiplicities are reported using the following abbreviations: s, singlet; d, doublet; dd, doublet of doublets; ddd, doublet doublet of doublets; dq, double quadrupet; dt, double of triplet; dtd, double triplet doublet; q, quadrupet; t, triplet; m, multiplet; br s, broad signal, * refers to interchangeable peaks. The accurate mass analyses were carried out using a LC/MSD-TOF spectrophotometer. HPLC-MS (Agilent 1260 Infinity II) analysis was conducted on a Poroshell 120 EC-C15 (4.6 mm × 50 mm, 2.7 μm) at 40 °C with mobile phase A (H_2O + 0.05 % formic acid) and B (ACN + 0.05 % formic acid) using a gradient elution and flow rate 0.6 mL/min. The DAD detector was set at 254 nm, the injection volume was 5 μL, and oven temperature was 40 °C. All tested compounds possess a purity of at least 95 %. The microwave oven used is BI-356006Biotage® Initiator + Microwave System EU, NET INTERLAB S.A.

*4.1.1. Diethyl ((1RS,3aRS,6aRS)-5-(3-chloro-4-fluorophenyl)-4,6-dioxo-1-phenyloctahydropyrrolo[3,4-c]pyrrol-1-yl)phosphonate hydrochloride (**B06-red. HCl**)*

To a solution of CH_3CN (3.7 mL) and H_2O (156 μL), **B06** (150 mg, 0.31 mmol) was added, and the mixture was stirred for 10 min. Then, $NaBH_3CN$ (39 mg, 0.62 mmol) and AcOH (156 μL) were added, and the mixture was stirred for 1 h at rt. The solvent was evaporated, EtOAc was added to the residue and the resulting solution was washed with a saturated solution of $NaHCO_3$. The organic phase was dried and concentrated. The crude was purified by column chromatography (EtOAc) and the residue was suspended in CH_2Cl_2 and a solution of HCl·EtOH 1.25 M to give **B06-red.HCl** (125 mg, 84 %) as a white solid. M.p. 125-127C (EtOAc). IR (NaCl) 3319, 2983, 2404, 1711, 1499, 1183, 1030, 960, 700 cm^{-1}. ^1H NMR (500 MHz, $CDCl_3$) δ 1.13 (t, $J = 7.0$ Hz, 3H, CH_2CH_3), 1.31 (t, $J = 7.0$ Hz, 3H, CH_2CH_3), 3.63 (td, $J = 8.0$, 2.5 Hz, 1H, H-3), 3.74 (dd, $J = 2.5$, 10.5 Hz, 1H, H-3), 3.78–3.88 (complex signal, 2H, H-3a and CH_2CH_3), 3.96–4.20 (m, 4H, CH_2CH_3 and H-6a), 6.61 (ddd, $J = 2.5$, 4.0, 9.0 Hz, 1H, ArH), 6.66 (dd, $J =$, 6.5, 2.5 Hz, 1H, ArH), 7.04 (t, $J = 8.5$ Hz, 1H, ArH), 7.30–7.41 (m, 3H, ArH), 7.74–7.83 (m, 2H, ArH).^{13}C NMR (126 MHz, $CDCl_3$) δ 16.2 (d, $J = 5.5$ Hz, CH_2CH_3), 16.4 (d, $J = 5.5$ Hz, CH_2CH_3), 48.1 (d, $J = 3.5$ Hz, C-3), 48.2

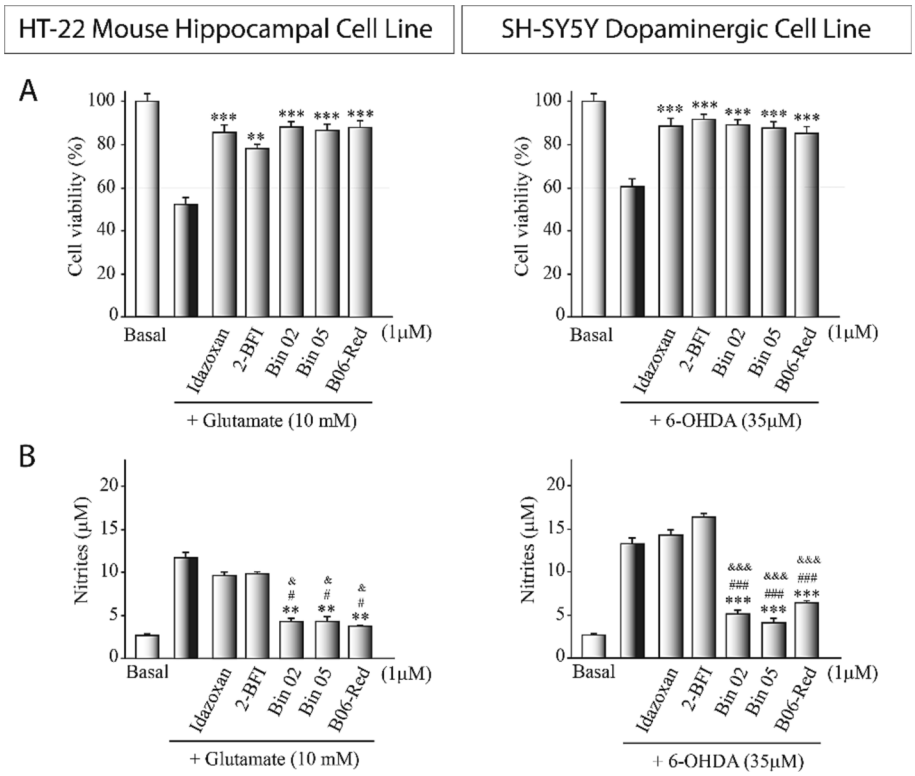

Fig. 7. *In vitro* I_2-IR ligand phenotypic screening: neuroprotective and anti-inflammatory effect. HT-22 hippocampal murine-derived and SH-SY5Y human dopaminergic cell lines were exposed to glutamate (10 μM) and 6-hydroxydopamine (6-OHDA, 35 μM), respectively, for 16 h. Previously, cultures were treated with the tested compounds at 1 μM. A) Cell viability was determined by MTT assay. B) Nitrite production was measured by the Griess reaction in the supernatant of the cells. Values represent the mean ± SD from triplicate determinations repeated at least three times. After confirming the significance of the results with an analysis of variance, a significance level of $p < 0.05$ was applied to the post hoc statistical analyses (Tukey test). $^{**}p \leq 0.01$, $^{***}p \leq 0.001$ versus glutamate- or 6-OHDA-treated cultures; $^{\#}$ $p \leq 0.05$, $^{\#\#\#}$ $p \leq 0.001$ versus idazoxan-treated cultures; $^{\&}$ $p \leq 0.5$, $^{\&\&\&}$ $p \leq 0.001$ versus 2-BFI-treated cultures.

(d, J = 3.5 Hz, C-3a), 52.5 (d, J = 3.5 Hz, C-6a), 63.5 (d, J = 8.0 Hz, CH_2CH_3), 64.2 (d, J = 7.5 Hz, CH_2CH_3), 69.8 (d, J = 149.5 Hz, C-1), 116.7 (d, J = 22.5 Hz, CHAr), 121.4 (d, J = 19.0 Hz, C-*ipso*), 126.2 (d, J = 7.5 Hz, CHAr), 127.8 (d, J = 4.0 Hz, CHAr), 128.0 (d, J = 2.0 Hz, 2CHAr), 128.3 (d, J = 4.5 Hz, 2CHAr), 128.7 (CHAr), 134.4 (d, J = 3.5 Hz, C-*ipso*), 156.6 (C-*ipso*), 158.6 (C-*ipso*), 173.5 (d, J = 9.0 Hz, CO), 176.6 (CO). HRMS $C_{22}H_{24}ClFN_2O_5P$ $[M + H]^+$ 481.1090; found, 481.1095.

4.1.2. Diethyl ((1RS,3RS,3aRS,6aRS)-3-(1H-indol-3-yl)-4,6-dioxo-5-phenyloctahydropyrrolo[3,4-c]pyrrol-1-yl)-1-phosphonate (*BIN01*)

To a mixture of **B02** (100 mg, 0.29 mmol) and $AgBF_4$ (83 mg, 0.43 mmol) in anhydrous THF (1.2 mL) under argon atmosphere was added a solution of indole (67 mg, 0.57 mmol) in anhydrous THF (2.6 mL). The mixture was stirred at room temperature for 24 h, and $AgBF_4$ (111 mg, 0.57 mmol) and indole (67 mg, 0.57 mmol) were added. Then, the reaction mixture was stirred for additional 48 h, filtered through a plug of Celite® with the aid of CH_2Cl_2, and washed with a saturated aqueous solution of NH_4Cl. The organic layer was dried, and the solvent evaporated. The resulting residue was purified by column chromatography (EtOAc/MeOH, 95:5) to afford **BIN01** (74 mg, 56 %) as grey foam. M.p. 156-158C (EtOAc). IR (NaCl) 3429, 2982, 1716, 1597, 1382 cm^{-1}. ^1H NMR (400 MHz, $CDCl_3$, COSY, HETCOR) δ 1.37 (t, J = 7.0 Hz, 3H, OCH_2CH_3), 1.41 (t, J = 7.0 Hz, 3H, OCH_2CH_3), 2.60 (br s, 1H, N*H*), 3.68 (dd, J = 9.5, 8.0 Hz, 1H, H-3a), 3.78 (t, J = 7.0 Hz, 1H, H-1), 3.96 (ddd, J = 18.0, 9.5, 7.0 Hz, 1H, H-6a), 4.24–4.32 (m, 4H, OCH_2CH_3), 4.59 (d, J = 8.0 Hz, 1H, H-3), 7.12 (m, 1H, ArH), 7.17 (m, 1H, ArH), 7.25–7.49 (m, 7H, ArH), 7.89 (d, J = 6.0 Hz, 1H, ArH), 8.53 (br s, 1H, NH). ^{13}C NMR (101 MHz) δ 16.4 (OCH_2CH_3), 16.5 (OCH_2CH_3), 48.6 (d, J = 2.0 Hz, C-6a), 52.6 (d, J = 7.5 Hz, C-3a), 57.0 (d, J = 165.5 Hz, C-1), 61.4 (d, J = 17.0 Hz, C-3), 63.1 (d, J = 6.5 Hz, OCH_2CH_3), 63.4 (d, J = 6.5 Hz, OCH_2CH_3), 111.5 (CHIn), 114.0 (C-2aIn), 119.7 (CHIn), 119.8 (CHIn), 122.4 (CHIn), 123.0 (CHIn), 125.6 (C2bIn), 126.4 (2CHAr), 128.7 (CHPh), 129.2 (2CHPh), 131.6 (C- *ipso*), 136.8 (C6aIn), 175.1 (CO), 175.3 (CO). MS-EI *m/z* 467 M^+ (23), 358 (24), 329 (100), 294 (15), 183 (33), 156 (34), 175 (11). HRMS $C_{24}H_{27}N_3O_5P$ $[M + H]^+$ 468.1684; found, 468.1683.

4.1.3. Diethyl ((1RS,3RS,3aRS,6aRS)-3-(1H-indol-3-yl)-4,6-dioxo-1,5-diphenyloctahydropyrrolo[3,4-c]pyrrole-1-yl)phosphonate (*BIN02*)

To a mixture of **B16** (50 mg, 0.117 mmol) and $AgBF_4$ (34 mg, 0.176 mmol) in anhydrous THF (2 mL) was added indole (27 mg, 0.23 mmol) under argon atmosphere. The mixture was stirred at room temperature for 48 h. Then, the solvent was evaporated under reduced pressure and the resulting residue was purified by column chromatography (CH_2Cl_2/MeOH, 99:1) to afford **BIN02** (54 mg, 85 %) as white solid. M.p. 123–125 °C (EtOAc). IR (NaCl) 3303, 2923, 1711, 1375, 1178, 1016, 970, 740, 702 690 cm^{-1}. ^1H NMR (400 MHz, $CDCl_3$, COSY, HETCOR) δ 1.15 (t, J = 7.0 Hz, 3H, OCH_2CH_3), 1.39 (t, J = 7.0 Hz, 3H, OCH_2CH_3), 3.57 (br s, 1H, N*H*), 3.88 (ddd, J = 9.5, 5.5, 1.0 Hz, 1H, H-3a), 3.94–4.18 (m, 2H, OCH_2CH_3), 4.31 (q, 2H, OCH_2CH_3), 4.47 (dd, J = 15.0, 9.5 Hz, 1H, H-6a), 5.27 (m, 1H, H-3), 6.54–6.76 (m, 2H, ArH), 7.16–7.26 (m, 2H, ArH), 7.28–7.34 (m, 4H, ArH), 7.34–7.46 (m, 4H, ArH), 7.78–7.95 (m, 2H, ArH), 8.01 (d, J = 8.5 Hz, 1H, ArH), 8.47 (br s, 1H, N*H*). ^{13}C NMR (101 MHz) δ 16.3 (d, J = 6.0 Hz, OCH_2CH_3), 16.6 (d, J = 6.0 Hz, OCH_2CH_3), 55.9 (d, J = 10.0 Hz, C-3a), 56.8 (C-6a), 58.2 (d, J = 15.0 Hz, C-3), 63.6 (d, J = 6.5 Hz, OCH_2CH_3), 64.6 (d, J = 7.5 Hz, OCH_2CH_3), 70.5 (d, J = 156.5 Hz, C-1), 111.8 (CHAr), 116.0 (C-*ipso*), 119.5 (CHAr), 120.2 (2CHAr), 122.4 (CHAr), 122.8 (CHAr), 125.4 (C- *ipso*), 126.7 (2CHAr), 128.2 (d, J = 4.0 Hz, 2CHAr), 128.4 (d, J = 2.0 Hz, CHAr),

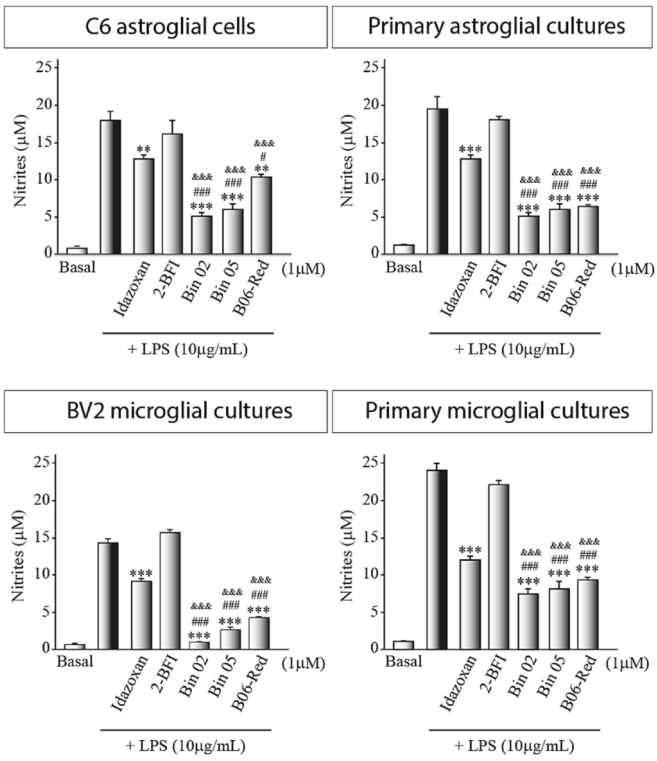

Fig. 8. *In vitro* anti-inflammatory effect of BIN02, BIN05 and B06-red. The Griess reaction was used to assess nitrite generation in the supernatant of glial cells after exposure during 24 h to lipopolysaccharide (LPS, 10 μg/mL) in the presence of the indicated compounds at 1 μM. Values represent the mean ± SD from triplicate determinations repeated at least three times. After confirming the significance of the results with an analysis of variance, a significance level of $p < 0.05$ was applied to the post hoc statistical analyses (Tukey test). $^{**}p \leq 0.01$, $^{***}p \leq 0.001$ versus LPS-treated cultures; $^{\#}p \leq 0.05$, $^{\#\#\#}p \leq 0.001$ versus idazoxan-treated cultures; $^{\&\&\&}p \leq 0.001$ versus 2-BFI-treated cultures.

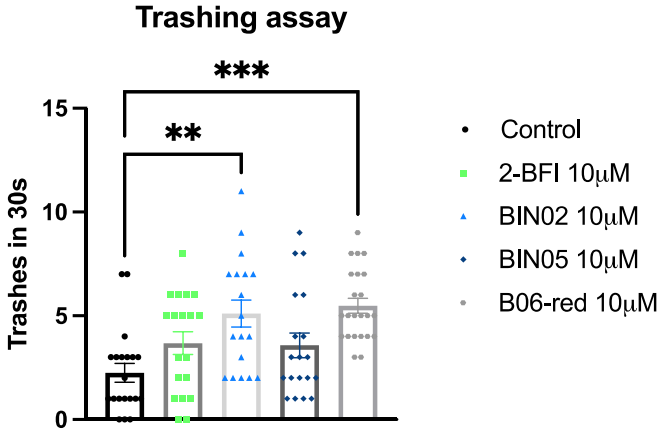

Fig. 9. Study of motility as estimated by thrashing assay (n = 20–30 worms/group; One-Way ANOVA and post-hoc Tukey's test:**$p < 0.01$;***$p < 0.001$). Values represented are mean ± SEM.

128.8 (2CHAr), 129.1 (2CHAr), 131.5 (C-*ipso*), 134.9 (C-*ipso*), 137.1 (C-*ipso*), 172.9 (CO), 176.2 (CO). HRMS $C_{30}H_{31}N_3O_5P$ $[M + H]^+$ 544.1996; found, 544.2006. Purity 96.41 % (t_R = 4.01).

4.1.4. Diethyl ((1RS,3aRS,6aRS)-5-(3-chloro-4-fluorophenyl)-3-(1H-indol-3-yl)-4,6-dioxo-1-phenyloctahydropyrrolo[3,4-c]pyrrol-1-yl) phosphonate ***(BIN05)***

To a mixture of **B06** (100 mg, 0.21 mmol) and $AgBF_4$ (61 mg, 0.31 mmol) in anhydrous THF (5 mL) under argon atmosphere was added indole (49 mg, 0.42 mmol). The mixture was stirred at room temperature for 48 h. Then, the solvent was evaporated under reduced pressure and the resulting residue was purified by column chromatography (CH_2Cl_2/MeOH, 99:1) to afford **BIN05** (80 mg, 64 %) as white solid. M.p. 144-147C (EtOAc). IR (ATR) 2989, 2925, 1713, 1496, 1377, 1237, 1168, 1018, 968, 742 cm^{-1}. ^1H NMR (400 MHz, $CDCl_3$) δ 1.15 (t, J = 7.0 Hz, 3H, OCH_2CH_3), 1.38 (t, J = 6.7 Hz, 3H, OCH_2CH_3), 3.56 (br s, 1H, N*H*), 3.83 (ddd, J = 9.5, 5.5, 1.0 Hz, 1H, H-3a), 3.97–4.12 (m, 2H, OCH_2CH_3), 4.23–4.36 (m, 2H, OCH_2CH_3), 4.44 (dd, J = 14.5, 9.5 Hz, 1H, H-6a), 5.29 (d, J = 6.5 Hz, 1H, H-3), 6.54–6.63 (m, 2H, ArH), 7.06 (t, J = 8.5 Hz, 1H, ArH), 7.16–7.28 (m, 2H, ArH), 7.30 (d, J = 2.5 Hz, 1H, ArH), 7.34–7.44 (m, 4H, ArH), 7.83–7.90 (m, 2H, ArH), 7.97 (d, J = 8.0 Hz, 1H, ArH), 8.51 (s, 1H, N*H*). ^{13}C NMR (101 MHz, $CDCl_3$) δ 16.3 (d, J = 6.0 Hz, OCH_2CH_3), 16.6 (d, J = 6.0 Hz, OCH_2CH_3), 55.8 (d, J = 10.0 Hz, C-3a), 56.8 (C-6a), 58.3 (d, J = 15.0 Hz, C-3), 63.6 (d, J = 6.5 Hz, OCH_2CH_3), 64.6 (d, J = 7.5 Hz, OCH_2CH_3), 70.6 (d, J = 156.5 Hz, C-1), 111.8 (CHAr), 115.9 (C-*ipso*), 116.8 (d, J = 22.5 Hz, CHAr), 119.4 (CHAr), 120.2 (CHAr), 121.5 (d, J = 19.0 Hz, C-*ipso*), 122.4 (CHAr), 122.8 (CHAr), 125.2 (C-*ipso*), 126.7 (d, J = 7.5 Hz, CHAr), 127.8 (d, J = 4.0 Hz, CHAr), 128.1 (d, J = 5.0 Hz, CHAr), 128.6 (d, J = 2.5 Hz, CHAr), 128.9 (d, J = 2.0 Hz, 2CHAr), 129.2 (CHAr), 134.9 (C-*ipso*), 137.2 (C-*ipso*), 156.7 (C-*ipso*), 159.2 (C-*ipso*), 172.5 (CO), 175.9 (CO). HRMS $C_{30}H_{29}ClFN_3O_5P$ $[M + H]^+$ 596.1512; found, 596.1525. Purity 98.21 % (t_R = 4.30).

4.1.5. Diethyl ((1RS,3aRS,6aRS)-5-(3-chlorophenyl)-3-(1H-indol-3-yl)-4,6-dioxo-1-phenyloctahydropyrrolo[3,4-c]pyrrol-1-yl)phosphonate ***(BIN06)***

To a mixture of **B53** (100 mg, 0.22 mmol) and $AgBF_4$ (63 mg, 0.33 mmol) in anhydrous THF (5 mL) under argon atmosphere was added indole (51.5 mg, 0.44 mmol). The mixture was stirred at room temperature for 48 h. Then, the solvent was evaporated under reduced pressure and the resulting residue was purified by column chromatography (CH_2Cl_2/MeOH, 99:1) to afford **BIN06** (75 mg, 59 %) as white solid. M.p. 159-161C (EtOAc). IR (ATR) 2973, 2925, 1713, 1372, 1230, 1163, 1016, 971, 744 cm^{-1}. ^1H NMR (400 MHz, $CDCl_3$) δ 1.15 (t, J = 7.0 Hz, 3H, OCH_2CH_3), 1.38 (t, J = 7.0 Hz, 3H, OCH_2CH_3), 3.58 (br s, 1H, N*H*), 3.85 (ddd, J = 9.5, 5.5, 1.0 Hz, 1H, H-3a), 4.00–4.11 (m, 2H, OCH_2CH_3), 4.26–4.36 (m, 2H, OCH_2CH_3), 4.45 (dd, J = 15.0, 9.5 Hz, 1H, H-6a), 5.29 (d, J = 5.5 Hz, 1H, H-3), 6.56–6.58 (m, 1H, ArH), 6.60 (dt, J = 7.5, 2.0 Hz, 1H, ArH), 7.16–7.29 (m, 4H, ArH), 7.31 (d, J = 2.5 Hz, 1H, ArH), 7.35–7.45 (m, 4H, ArH), 7.84–7.91 (m, 2H, ArH), 7.99 (d, J = 8.5 Hz, 1H, ArH), 8.49 (s, 1H, N*H*). ^{13}C NMR (101 MHz, $CDCl_3$) δ 16.1 (d, J = 6.0 Hz, OCH_2CH_3), 16.5 (d, J = 6.0 Hz, OCH_2CH_3), 55.7 (d, J = 10.0 Hz, C-3a), 56.7 (C-6a), 58.2 (d, J = 15.0 Hz, C-3), 63.4 (d, J = 7.0 Hz, OCH_2CH_3), 64.5 (d, J = 7.5 Hz, OCH_2CH_3), 70.4 (d, J = 156.5 Hz, C-1), 111.7 (2CHAr), 115.8 (C-*ipso*), 119.3 (CHAr), 120.1 (CHAr), 122.2 (CHAr), 122.7 (CHAr), 124.8 (CHAr), 125.1 (C-*ipso*), 127.0 (CHAr), 128.0 (d, J = 5.0 Hz, 2CHAr), 128.4 (d, J = 3.0 Hz, CHAr), 128.8 (d, J = 8.5 Hz, 2CHAr), 129.8 (CHAr), 132.4 (C-*ipso*), 134.4 (C-*ipso*), 134.7 (C-*ipso*), 137.0 (C-*ipso*), 172.4 (CO), 175.8 (CO). HRMS $C_{30}H_{29}ClN_3O_5P$ $[M + H]^+$ 578.1606; found, 578.1605.

4.1.6. (2RS,3RS)-2-(1H-indol-3-yl)-N,5-diphenyl-3,4-dihydro-2H-pyrrole-3-carboxamide ***(PIP-BIN02)***

A solution of **BIN02** (240 mg, 0.44 mmol) in 0.05 M NaOH in THF/H_2O 2:1 (12 mL) was stirred at room temperature for 2.5 h. The mixture was concentrated *in vacuo*, water (2 mL) was added, and the pH of the mixture was acidified (pH = 3) with a 1 M solution of HCl. The reaction mixture was extracted with EtOAc, the organic phases were combined, dried, filtered, and concentrated to give a residue that was purified by column chromatography (CH_2Cl_2) to afford **PIP-BIN02** (132 mg, 80 %) as a white solid. M.p. 148-149C (EtOAc). IR 3344, 2989, 2926, 1712, 1379, 1229, 1180, 1017, 974, 741, 703 (ATR) cm^{-1}. ^1H NMR [500 MHz, DMSO] δ 3.27–3.36 (m, 1H, H-4), 3.47 (dt, J = 9.5, 7.5 Hz, 1H, H-3),

3.64 (ddd, J = 17.0, 9.5, 2.0 Hz, 1H, H-4), 5.68 (d, J = 6.5 Hz, 1H, 2-H), 6.92 (ddd, J = 8.0, 7.0, 1.0 Hz, 1H, ArH), 7.01–7.11 (m, 2H, ArH), 7.25–7.34 (m, 3H, ArH), 7.39 (dd, J = 16.5, 8.0 Hz, 2H, ArH), 7.43–7.53 (m, 3H, ArH), 7.61 (dd, J = 8.5, 1.0 Hz, 2H, ArH), 7.92 (dd, J = 8.0, 1.5 Hz, 2H, ArH), 10.08 (s, 1H, NH), 10.97 (s, 1H, NH).^{13}C NMR (126 MHz, $(CD_3)_2SO$) δ 40.4 (C-4), 50.6 (C-3), 73.5 (C-2), 111.0 (CHAr), 116.1 (*C-ipso*), 117.9 (CHAr), 118.4 (CHAr), 118.7 (2CHAr), 120.5 (CHAr), 121.8 (CHAr), 122.7 (CHAr), 125.4 (*C-ipso*), 127.2 (2CHAr), 128.0 (2CHAr), 128.1 (2CHAr), 130.0 (CHAr), 133.3 (*C-ipso*), 136.1 (*C-ipso*), 138.5 (*C-ipso*), 168.7 (CO), 172.3 (C-5). HRMS $C_{25}H_{22}N_3O$ $[M + H]^+$ 380.1754; found, 380.1757. Purity 100 % (t_R = 3.35 min).

*4.1.7. Tetraethyl (1RS,3aSR,6aRS,1′SR,3′RS,3a'SR,6a'SR)-5,5′-diphenyl-4,4′,6,6′-tetraoxo- 1,1′,2′,3′,3a,3a',4,4′,5,5′,6,6′,6a,6a'-tetradecahydrobipyrrolo[3,4-c]pyrrole-1,1′-diphosphate (**BxB03 and BxB04,** Table 2, entry 3).*

To a solution of **B02** (80 mg, 0.23 mmol) in anhydrous CH_2Cl_2 (1 mL) was added TMSCl (149 mg, 1.37 mmol). The mixture was stirred under microwave irradiation at 80 °C and 250 bar, for 30 min. The solvent was evaporated under reduced pressure and the residue was purified by silica gel flash chromatography (EtOAc/MeOH, 95:5) to afford **BxB03** (20 mg, 25 %), **BxB04** (34 mg, 43 %) and **B02** (13 mg, 16 %). **BxB03:** IR (NaCl) 3267, 2984, 1705, 1434 cm^{-1}. ^{1}H NMR (400 MHz, $CDCl_3$, COSY, HETCOR) δ 1.33 (t, J = 7.0 Hz, 3H, OCH_2CH_3), 1.41 (dq, J = 14.0, 7.0 Hz, 9H, OCH_2CH_3), 2.74 (br s, 1H, NH), 3.69 (m, 1H, H-1′), 3.86 (ddd, J = 18.5, 9.5, 7.5 Hz, 1H, H-6a'), 4.10–4.41 (complex signal, 10H, OCH_2CH_3, H-3a' and H-6a), 4.62 (t, J = 6.5 Hz, 1H, H-3′), 4.82 (ddd, J = 22.5, 4.0, 3.0 Hz, 1H, H-1), 7.24 (d, J = 1.5 Hz, 1H, ArH), 7.27–7.31 (m, 2H, ArH), 7.37–7.51 (m, 7H, ArH), 7.81 (dd, J = 4.0, 3.0 Hz, 1H, H-3). ^{13}C NMR (101 MHz) δ 16.5 (m, OCH_2CH_3), 45.3 (C-3a'), 47.5 (C-6a'), 48.1 (d, J = 7.0 Hz, C-6a), 57.0 (d, J = 175.0 Hz, C-1′), 62.5 (d, J = 14.5 Hz, C-3′), 63.3 (d, J = 7.0 Hz, OCH_2CH_3), 63.6 (d, J = 7.0 Hz, OCH_2CH_3), 63.8 (d, J = 7.5 Hz, OCH_2CH_3), 64.5 (d, J = 6.5 Hz, OCH_2CH_3), 73.8 (d, J = 159.5 Hz, C-1), 74.7 (C-3a), 126.4 (2CHAr), 126.5 (2CHAr), 128.9 (CHAr), 129.2 (CHAr), 129.3 (2CHAr), 129.4 (2CHAr), 131.2 (C-*ipso*), 131.6 (C-*ipso*), 164.8 (d, J = 14.0 Hz, C-3), 174.0 (d, J = 5.5 Hz, CO), 174.7 (d, J = 5.5 Hz, CO), 175.2 (d, J = 12.0 Hz, CO), 175.7 (CO). HRMS $C_{32}H_{37}N_4O_{10}P_2$ $[M + H]^+$ 701.2136; found, 701.2126. **BxB04:** IR (NaCl) 3267, 2984, 1705, 1434 cm^{-1}. ^{1}H NMR (400 MHz, $CDCl_3$, COSY, HETCOR) δ 1.26 (t, J = 7.0 Hz, 3H, OCH_2CH_3), 1.31–1.44 (m, 9H, OCH_2CH_3), 3.20 (br s, 1H, NH), 3.62 (m, 1H, H-1′), 3.81 (ddd, J = 18.0, 10.0, 8.0 Hz, 1H, H-6a'), 3.92 (dd, J = 7.0, 5.0 Hz, 1H, H-3′), 4.14 (m, 1H, H-6a), 4.16–4.33 (m, 8H, OCH_2CH_3), 4.57 (dd, J = 9.5, 7.5 Hz, 1H, H-3a'), 4.89 (dt, J = 22.0, 3.0 Hz, 1H, H-1), 7.21–7.29 (m, 4H, ArH), 7.40 (m, 2H, ArH), 7.45 (m, 4H, ArH), 8.04 (dd, J = 4.5, 3.0 Hz, 1H, H-3).^{13}C NMR (101 MHz) δ 16.5 (OCH_2CH_3), 16.61 (OCH_2CH_3), 46.8 (C-6a'), 47.4–47.5 (C-3a'*and C-6a*), 56.6 (d, J = 173.5 Hz, C-1′), 63.1 (d, J = 6.5 Hz, OCH_2CH_3), 63.8 (d, J = 16.5 Hz, C-3′), 63.9 (d, J = 6.5 Hz, OCH_2CH_3), 64.3 (d, J = 6.5 Hz, OCH_2CH_3), 70.9 (C-3a), 74.7 (d, J = 160.0 Hz, C-1), 126.5 (2CHAr), 126.5 (2CHAr), 129.0 (CHAr), 129.2 (CHAr), 129.3 (2CHAr), 129.4 (2CHAr), 131.1 (C-*ipso*), 131.5 (C-*ipso*), 164.4 (d, J = 13.0 Hz, C-3), 173.7 (d, J = 6.0 Hz, CO), 174.5 (d, J = 4.5 Hz, CO), 174.7 (d, J = 11.5 Hz, CO), 175.6 (CO). HRMS $C_{32}H_{37}N_4O_{10}P_2$ $[M + H]^+$ 701.2136; found, 701.2131.

*4.1.8. Tetraethyl (1RS,3aSR,6aRS,1′SR,3′RS,3a'SR,6a'SR)-5,5′-dimethyl-4,4′,6,6′-tetraoxo- 1,1′,2′,3′,3a,3a',4,4′,5,5′,6,6′,6a,6a'-tetradecahydrobipyrrolo[3,4-c]pyrrole-1,1′- diphosphate (**BxB01 and BxB02,** Table 2, entry 7).*

To a solution of **B03** (100 mg, 0.346 mmol) in anhydrous CH_2Cl_2 (1 mL) was added TMSCl (225.61 mg, 2.08 mmol). The mixture was stirred under microwave irradiation at 80 °C and 250 bar for 30 min. The solvent was evaporated under reduced pressure and the residue was purified by silica gel flash chromatography (EtOAc/MeOH, 95:5) to afford **BxB01** (24 mg, 24 %), **BxB02** (34 mg, 34 %) and **B03** (3 mg, 3 %). **BxB01:** IR (NaCl) 3466, 2984, 1705, 1435 cm^{-1}. ^{1}H NMR (400 MHz, $CDCl_3$, COSY, HETCOR) δ ^{1}H NMR (400 MHz, $CDCl_3$) δ 1.34 (dt, J = 7.0, 14.0 Hz, 9H, OCH_2CH_3), 1.42 (t, J = 7.0 Hz, 3H, OCH_2CH_3), 2.53 (br s, 1H, NH), 2.94 (s, 3H, NCH_3), 2.96 (s, 3H, NCH_3), 3.46 (m, 1H, H-1′), 3.61 (ddd, J = 17.5, 9.0, 8.0 Hz, 1H, H-6a'), 3.91 (dd, J = 18.5, 4.0 Hz, 1H, H-6a), 3.97 (m, 1H, H-3a'), 4.21 (dtd, J = 31.0, 14.5, 7.0 Hz, 8H, OCH_2CH_3), 4.33 (m, 1H, H-3′), 4.64 (dt, J = 22.5, 3.5, Hz 1H, H-1), 7.69 (m, 1H, H-3). ^{13}C NMR (101 MHz) δ 16.5 (d, J = 6.0 Hz, OCH_2CH_3), 16.6 (d, J = 6.0 Hz, OCH_2CH_3), 25.3 (NCH_3), 25.6 (NCH_3), 45.2 (C-6a), 47.3 (C-6a'), 47.9 (d, J = 7.5 Hz, C-3a'), 56.5 (d, J = 174.5 Hz, C-1′), 61.5 (d, J = 15.5 Hz, C-3′), 63.2 (d, J = 7.0 Hz, OCH_2CH_3), 63.5 (d, J = 7.0 Hz, OCH_2CH_3), 63.6 (d, J = 7.5 Hz, OCH_2CH_3), 64.4 (d, J = 6.5 Hz, OCH_2CH_3), 73.3 (d, J = 160.0 Hz, C-1), 74.7 (C-3a), 164.8 (d, J = 13.5 Hz, C-3), 174.8 (d, J = 5.5 Hz, CO), 175.6 (d, J = 5.0 Hz, CO), 176.1 (d, J = 12.0 Hz, CO), 176.6 (CO). HRMS $C_{22}H_{35}N_4O_{10}P_2$ $[M + H]^+$ 577.1823; found, 577.1820. **BxB02:** IR (NaCl) 3267, 2984, 1698, 1434 cm^{-1}. ^{1}H NMR (400 MHz, $CDCl_3$, COSY, HETCOR) δ 1.32–1.39 (m, 9H, OCH_2CH_3), 1.42 (t, J = 7.5 Hz, 3H, OCH_2CH_3), 1.82 (br s, 1H, NH), 2.93 (br s, 1H, NCH_3), 2.94 (br s, 1H, NCH_3), 3.40 (ddd, J = 8.0, 5.0, 3.5 Hz, 1H, H1′), 3.54–3.67 (complex signal, 2H, H-6a' and H-3a'), 4.02 (dd, J = 18.0, 3.5 Hz, 1H, H-6a), 4.17–4.33 (complex signal, 9H, H-3′ and OCH_2CH_3), 4.72 (ddd, J = 22.0, 3.5, 2.5 Hz, 1H, H-1), 7.92 (dd, J = 4.5, 2.5 Hz, 1H, H-3).^{13}C NMR (101 MHz) δ 16.6 (d, J = 5.5 Hz, OCH_2CH_3), 16.7 (d, J = 5.5 Hz, OCH_2CH_3), 25.3 (NCH_3), 25.5 (NCH_3), 46.3 (d, J = 8.0 Hz, C-3a'), 47.5 (C-6a'), 47.4 (d, J = 9.5 Hz, C-6a), 56.2 (d, J = 174.0 Hz, C-1′), 63.1 (d, J = 4.5 Hz, OCH_2CH_3), 63.2 (d, J = 16.0 Hz, H-3′), 63.7 (d, J = 7.0 Hz, OCH_2CH_3), 63.8 (d, J = 6.5 Hz, OCH_2CH_3), 64.2 (d, J = 6.5 Hz, OCH_2CH_3), 71.1 (C-3a), 74.1 (d, J = 160.5 Hz, C-1), 164.4 (d, J = 13.5 Hz, C-3), 174.7 (d, J = 5.5 Hz, CO), 175.5 (d, J = 3.5 Hz, CO), 175.6 (d, J = 12.0 Hz, CO), 176.6 (CO). HRMS $C_{22}H_{36}N_4O_{10}P_2$ $[M + H]^+$ 577.1823; found, 577.1814.

*4.1.9. Tetraethyl (1RS,3aSR,6aRS,1′SR,3′RS,3a'SR,6a'SR)-4,4′,6,6′-tetraoxo-1′,3,5,5′-tetraphenyl-1,1′,2′,3′,3a,3a',4,4′,5,5′,6,6′,6a,6a'-tetradecahydrobipyrrolo[3,4-c]pyrrole-1,1′- diphosphate (**BxB05 and BxB06**).*

To a solution of **B16** (541 mg, 1.27 mmol) in anhydrous CH_2Cl_2 (7.5 mL) was added TMSCl (0.96 mL, 7.61 mmol). The mixture was stirred under microwave irradiation at 80 °C and 250 bar for 30 min. The solvent was evaporated under reduced pressure and the residue was purified by silica gel flash chromatography (EtOAc/MeOH, 95:5) to afford **BxB05** (292 mg, 27 %), **BxB06** (444 mg, 41 %) and **B16** (81 mg, 15 %). **BxB05:** IR (ATR) 3469, 2988, 2920, 1710, 1494, 1383, 1192, 1034, 1016, 963, 775, 732, 691 cm^{-1}.^{1}H NMR (400 MHz, $CDCl_3$, COSY, HETCOR) δ 1.21 (dt, J = 9.5, 7.0 Hz, 6H, OCH_2CH_3), 1.36 (t, J = 7.0 Hz, 3H, OCH_2CH_3), 1.45 (t, J = 7.0 Hz, 3H, OCH_2CH_3), 2.86 (d, J = 5.5 Hz, 1H, NH), 3.92–4.07 (m, 1H, OCH_2CH_3), 4.10–4.24 (m, 5H, OCH_2CH_3), 4.25–4.43 (complex signal, 5H, OCH_2CH_3, H-6a, H-6a' and H-3a'), 5.28 (m, 1H, H-3′), 6.48 (ddd, J = 17.0, 6.5, 3.0 Hz, 4H, ArH), 7.27 (d, J = 2.0 Hz, 6H, ArH), 7.36 (t, J = 5.0 Hz, 6H, ArH), 7.52–7.63 (m, 2H, ArH), 7.67 (d, J = 7.5 Hz, 2H, ArH), 8.16 (d, J = 3.5 Hz, 1H, H-3). ^{13}C NMR (101 MHz) δ 16.4 (d, J = 5.5 Hz, $2OCH_2CH_3$), 16.6 (t, J = 5.0 Hz, $2OCH_2CH_3$), 49.1 (d, J = 9.5 Hz, C-3a'), 51.6 (C-6a), 53.8 (C-6a'), 60.6 (d, J = 14.0 Hz, C-3′), 63.5 (d, J = 7.5 Hz, OCH_2CH_3), 64.5 (t, J = 7.0 Hz, OCH_2CH_3), 64.8 (d, J = 7.0 Hz, OCH_2CH_3), 67.0 (d, J = 172.0 Hz, C-1′), 76.0 (C-3a), 85.5 (d, J = 161.5 Hz, C-1), 126.2 (2CHAr), 126.4 (2CHAr), 127.4 (d, J = 5.0 Hz, 2CHAr), 128.2 (2CHAr), 128.5 (d, J = 5.5 Hz, 2CHAr), 128.8 (d, J = 6.0 Hz, 2CHAr), 128.9 (2CHAr), 129.0 (2CHAr), 129.1 (2CHAr), 129.2 (2CHAr), 131.2 (d, J = 5.0 Hz, 2C-*ipso*), 134.1 (d, J = 4.5 Hz, C-*ipso*), 135.8 (d, J = 6.5 Hz, C-*ipso*), 164.4 (d, J = 14.0 Hz, C-3), 171.5 (d, J = 7.5 Hz, CO), 172.3 (CO), 173.7 (d, J = 4.5 Hz, CO), 175.8 (CO). HRMS $C_{44}H_{47}N_4O_{10}P_2$ $[M + H]^+$ 853.2762; found, 853.2761. Purity 95.77 % (t_R = 4.77). **BxB06:** IR (ATR) 3247, 2976, 2932, 1704, 1497, 1383, 1365, 1252, 1227, 1026, 965, 796, 703 cm^{-1}.^{1}H NMR (400 MHz, $CDCl_3$, COSY, HETCOR) δ 1.19–1.33 (m, 12H, OCH_2CH_3), 3.42 (d, J = 5.0 Hz, 1H, NH), 4.04–4.16 (m, 3H, OCH_2CH_3), 4.16–4.30 (m, 5H, OCH_2CH_3), 4.30–4.43 (complex signal, 2H, H-6a and

H-6a'), 4.50 (t, $J = 5.5$ Hz, 1H, H-3′), 4.70 (dd, $J = 9.5$, 5.0 Hz, 1H, H-3a'), 6.56 (dd, $J = 6.5$, 3.0 Hz, 2H, ArH), 6.65 (dd, $J = 6.5$, 3.0 Hz, 2H, ArH), 7.29 (d, $J = 3.0$ Hz, 6H, ArH), 7.33–7.41 (m, 6H, ArH), 7.56–7.71 (m, 4H, ArH), 8.32 (d, $J = 4.0$ Hz, 1H, H-3). ^{13}C NMR (101 MHz) δ 16.4 (d, $J = 7.0$ Hz, 2OCH$_2$*C*H$_3$), 16.6 (d, $J = 5.5$ Hz, 2OCH$_2$*C*H$_3$), 49.5 (d, $J = 10.5$ Hz, C-3a'), 53.3 (d, $J = 2.5$ Hz, C-6a'), 53.9 (C-6a), 61.7 (d, $J = 15.0$ Hz, C-3′), 63.7 (d, $J = 7.5$ Hz, O*C*H$_2$CH$_3$), 64.2 (d, $J = 7.5$ Hz, O*C*H$_2$CH$_3$), 64.5 (d, $J = 7.0$ Hz, O*C*H$_2$CH$_3$), 65.3 (d, $J = 7.0$ Hz, O*C*H$_2$CH$_3$), 69.0 (d, $J = 168.0$ Hz, C-1′), 72.5 (C-3a), 86.6 (d, $J = 160.5$ Hz, C-1), 126.4 (d, $J = 18.0$ Hz, CHAr), 127.6 (d, $J = 4.5$ Hz, CHAr), 128.3 (CHAr), 128.5 (d, $J = 5.5$ Hz, CHAr), 128.8 (d, $J = 14.5$ Hz, CHAr), 129.1 (d, $J = 2.5$ Hz, CHAr), 131.3 (d, $J = 21.5$ Hz, 2*C-ipso*), 133.7 (d, $J = 3.5$ Hz, *C-ipso*), 135.1 (d, $J = 4.5$ Hz, *C-ipso*), 164.1 (d, $J = 13.5$ Hz, C-3), 171.1 (d, $J = 8.0$ Hz, CO), 172.6 (CO), 173.3 (d, $J = 4.5$ Hz, CO), 175.7 (CO). HRMS $C_{44}H_{47}N_4O_{10}P_2$ $[M + H]^+$ 853.2762; found, 853.2758.

4.2. X-ray crystallographic analysis

Crystals of **B24-red**, **BIN05**, **PIP-BIN02**, **BxB05** and **BxB06** were obtained from slow evaporation of methanol solutions. The single crystal X-Ray diffraction data set was collected at 294 K up to a max 2ϑ of ca. 57° on a Bruker Smart APEX II diffractometer, using monochromatic MoKα radiation λ = 0.71073 Å and 0.3° separation between frames. Data integration was performed using SAINT V6.45A and SORTAV (Blessing, 1995) in the diffractometer package. The crystal and collection data and structural refinement parameters are given in the Tables in the supplementary data. The structures were solved by direct methods using SHELXT-2014 and Fourier's difference methods and refined by least squares on F2 using SHELXL-2014/7 inside the WinGX program environment [54,55]. Anisotropic displacement parameters were used for non-H atoms and the H-atoms were positioned in calculated positions and refined riding on their parent atoms. Atom coordinates are given and bond distances and hydrogen bonds. All this information is detailed in the Tables in the supplementary data.

B24-red crystallized in the monoclinic *P*21/a space group (Ortep in Scheme 1). The cyclohexane ring presents some orientational disorder (8 %) that has been modelled. The pyrrolidine ring presents an envelope conformation on N2, while the other pyrrolidine is flat. All the stereocenters (C1, C3a, C6a) exhibit the same quirality, either S or R, depending on the molecule in the crystal, as the space group is centrosymmetric. Molecules are connected through the N2-H2···O1 hydrogen bond (HB).

BIN05 crystallized in the triclinic *P*-1 space group (Ortep in Scheme 2). The pyrrolidine rings present envelope conformations on C1 and *C*2, respectively. The remaining rings appears as flat. The stereocenters C1, *C*2, C5, C6 exhibit quiralities either S,R,R,R, respectively, or, R,S,S,S, respectively. Molecules are packed in dimers through the mutual N53-H53···O1 HB.

PIP-BIN02 crystallized in the monoclinic *C*2/*c* space group with a water molecule (Ortep in Scheme 3). The rings are planar and the two stereocenters show identical quirality, either S,S or R,R. The water molecule binds to three molecules by the HB: N23-H23···O1, O1-H1···O6, O1-H2···N1.

BxB05 crystallized in the triclinic *P*-1 space group with two water molecules (Ortep in Fig. 4). In this case, the four pyrrolidine rings present twisted conformations on C1-C6a, on C3a-C6a, on N2′-C1′ and on C6a'-C6′, respectively. One pyrrolidine shows R,R,S quiralities at the C1, C3a, C6a centers, while the other presents R,S,S quiralities at the C1′, C3a', C6a' sites. C3′ exhibits a S quirality. Due to the centrosymmetry of the space group, the crystal is racemic, and the fully inverted molecule is also equally present. The two water molecules bridge between themselves and with oxygens of the phosphonates through HB.

BxB06 crystallized in the monoclinic *Cc* space group with two molecules per asymmetric unit (Ortep in Fig. 4). Two pyrrolidines are twisted (on C1-C6a and on N2′-C1′), one is envelope on C6′, while the other appears as flat. The Flack parameter (0.04(12)) confirms the absolute configuration of the solved crystal structure, but it is observed that the two independent molecules exhibit inverse quiralities at all quiral centers. Thus, also in these cases, both fully inverted molecules are equally present in the crystal. One pyrrolidine shows R,R,S quiralities at the C1, C3a, C6a centers, while the other presents S,R,R quiralities at the C1′, C3a', C6a' sites. C3′ exhibits a R quirality. Both independent molecules are linked in pairs by several HB. The quirality of the crystal is however an effect of the packing and not due the quirality of the molecules themselves. In fact, this is not uncommon.

Crystallographic data for the reported structures has been deposited in the Cambridge Crystallographic Data Centre as supplementary publication, CCDC No. **B24-red** (2250189), **BIN05** (2250193), **PIP-BIN02** (2250192), **BxB05** (2250191) and **BxB06** (2250190). Copies of this information may be obtained free of charge from The Director, CCDC, 12 Union Road, Cambridge CB2 1EZ, UK. Fax: þ44 1223 336 033. data_request@ccdc.cam.ac.uk. Web page: https://www.ccdc. cam.ac.uk.

4.3. Binding studies

4.3.1. Preparation of cellular membranes

Human brain samples were obtained at autopsy in the Basque Institute of Legal Medicine, Bilbao, Spain. Samples from the prefrontal cortex (Brodmann's area 9) were dissected at the time of autopsy and immediately stored at −70 °C until assay. The study was developed in compliance with policies of research and ethical review boards for postmortem brain studies.

To obtain cellular membranes (*P*2 fraction) the different samples were homogenized using an ultraturrax in 10 volumes of homogenization buffer (0.25 M sucrose, 5 mM Tris–HCl, pH 7.4). The crude homogenate was centrifuged for 5 min at 1000 g (4 °C) and the supernatant was centrifuged again for 10 min at 40,000 g (4 °C). The resultant pellet was washed twice in 5 volumes of homogenization buffer and recentrifuged in similar conditions. Protein content was measured according to the method of Bradford using BSA as standard.

4.3.2. Competition binding assays

The pharmacological activity of the compounds was evaluated through competition binding studies against the I_2-IR selective radioligand [^{3}H]2-BFI or the α_2-adrenergic receptor selective radioligand [^{3}H]RX821002. Specific binding was measured in 0.25 mL aliquots (50 mM Tris-HCl, pH 7.5) containing 100 μg of membranes, which were incubated in 96-well plates either with [^{3}H]2-BFI (2 nM) for 45 min at 25 °C or [^{3}H]RX821002 (1 nM) for 30 min at 25 °C, in the absence or presence of the competing compounds (10^{-12} to 10^{-3} M, 10 concentrations).

Incubations were terminated by separating free ligand from bound ligand by rapid filtration under vacuum (1450 Filter Mate Harvester, PerkinElmer) through GF/C glass fiber filters. The filters were then rinsed three times with 300 μL of binding buffer, air-dried (120 min), and counted for radioactivity by liquid scintillation spectrometry using a MicroBeta TriLux counter (PerkinElmer). Specific binding was determined and plotted as a function of the compound concentration. Nonspecific binding was determined in the presence of idazoxan (10^{-5} M), a compound with well stablished affinity for I_2-IR and α_2-adrenergic receptors, in [^{3}H]2-BFI and [^{3}H]RX821002 assays. To obtain the inhibition constant (K_i) analyses of competition experiments were performed by nonlinear regression using the GraphPad Prism program. K_i values were normalized to pK_i values. I_2-IR/α_2 selectivity index was calculated as the antilogarithm of the difference between pK_i values for I_2-IR and pK_i values for α_2-AR.

4.4. Cellular models of Alzheimer's and Parkinson's diseases

4.4.1. In vitro model of neurodegeneration

4.4.1.1. Cell lines and treatments. The HT-22 mouse hippocampal neuronal cell line has been recognized as a valuable cell model for the study of neurotoxicity associated with AD. HT-22 cultures (Merck-Sigma Aldrich, SCC129) were maintained in DMEM-F12 (Gibco) containing 10 % (v/v) fetal bovine serum (FBS), 100 U/mL penicillin and 100 μg/mL streptomycin.

The SH-SY5Y cell line has been a valuable asset to help unravel the molecular complexity of PD. Cells were purchased from American Type Culture Collection (ATCC, Rockville, MD, Ref.CRL-2266) and grown in RPMI medium (Gibco) supplemented with glutamine (2 mM), 10 % FBS and 1 % penicillin/streptomycin.

Cell lines were cultured under standard conditions (37 °C, 5 %CO_2). On attaining semiconfluence, cells were seeded on 96-well plates at $3x10^4$ per well and incubated for 24 h prior to treatment. Then, cells were treated with the indicated compounds for 24 h and viability was assessed using the MTT assay. None of the compounds tested were cytotoxic at those doses Then, HT-22 and SH-SY5Y cultures were treated for 1 h with the compounds at 1 μM. This dose was chosen based on previous studies [28]. After that, glutamate (10 mM, Merck-Sigma) was added to the HT-22 cultures, and 6-hydroxydopamine (6-OHDA, 35 μM, Merck-Sigma) to the SH-SY5Y cultures, that were incubated for at least 16 h. As a final step, cultures were tested for viability and nitrite production.

4.4.1.2. Cell viability assay. Cell viability was assessed using 3-(4,5-dimethylthiazol-2-yl)-5-(3-carboxymethoxyphenyl)-2-(4-sulfophenyl)–2*H*-tetrazolium (MTT) assay, according to manufacturer's instructions (Roche Diagnostic). Briefly, after exposure to glutamate or 6-OHDA cell culture medium was replaced with 100 μL of fresh culture medium added with MTT solution (0.5 mg/mL) for 1 h. Medium was removed and the resulting formazan crystals were dissolved in DMSO and the absorbance read at 595–650 nm in a spectrophotometer. All experiments were performed at least three times and the results were expressed as a percentage of the control.

4.4.2. In vitro model of neuroinflammation

4.4.2.1. Cell lines and treatments. The brain-derived rat C6 astroglia-like cell line (ATCC; CCL-107) was cultured in DMEM with 10 % FBS and 1 % penicillin/streptomycin in a humidified atmosphere containing 5 % CO_2 in air at 37 °C in an incubator. Cell line of murine BV2 microglia was maintained at 37 °C in DMEM added with 1 % of 100 U/mL of penicillin/streptomycin and 10 % fetal bovine serum in a humidified incubator containing 5 % CO_2. C6 and BV2 cells were cultured until 80–90 % confluent in 75 cm2 flasks. To determine the inflammatory state, cells were further sub-cultured in 96-well plates at a density of $3x10^4$/well. Now, cultures were pre-treated for 1 h with the compounds **BIN02**, **BIN05** and **B06-red** at 1 μM. Then, lipopolysaccharide (10 μg/mL, Sigma) was added to the medium and cultures incubated for 24 h. Finally, nitrite production was evaluated.

4.4.2.2. Cell lines and treatments. Mouse primary astrocytes and microglia were harvested and cultured as previously described [56]. Briefly, after removal of the meninges the cerebral cortex was dissected, dissociated, and incubated with 0.25 % trypsin, EDTA at 37 °C for 1 h. Tissue was then centrifugated and the resulting pellet washed with Hanks' balanced salt solution (HBSS, Invitrogen). Cells were plated on non-coated flasks and incubated in standard conditions for at least 7 days. Now, each glial type was then isolated to create pure cultures. To that end, glial cells on culture flasks were agitated on an orbital shaker for 4 h at 240 rpm at 37 °C, the supernatant was collected, centrifuged, and the cellular pellet containing the microglial cells resuspended in complete medium (HAMS/DMEM (1:1) containing 10 % FBS) and seeded on uncoated 96-well plates. Cells were allowed to adhere for 2 h, and the medium was removed to eliminate nonadherent oligodendrocytes. New fresh medium containing 10 ng/mL of GM-CSF was added. The remaining astroglial cells adhered to the flasks were then trypsinized, collected, centrifuged, and plated onto 96-well plates with complete medium. As determined by immunofluorescence with antibodies to Iba-1 (microglial marker) and GFAP (astrocyte marker), cultures obtained by this procedure were > 98 % pure. Afterwards, cells were treated with compounds (1 μM) for 1 h, followed by LPS (10 μg/mL) for 24 h. Then, nitrite production was measured.

4.4.2.3. Inflammation determination: Nitrites measurement. SH-SY5Y, HT-22, C6, BV2 and glial primary cultures seeded in 96-well plates were used. After treatments, cell culture supernatant (100 μL) was mixed to an equal volume of Griess reagent (1 % sulfanylamide and 0.1 % naphthyl ethylene diamine in 5 % phosphoric acid; Sigma-Aldrich) at room temperature for 15 min. Standard solution of sodium nitrite was used to determine nitrite concentrations. The absorbance was read at 492/540 nm using a microplate reader (Thermofischer). All experiments were performed at least three times.

4.5. In vivo Caenorhabditis elegans study

4.5.1. Study design

The overall objective of the study was to evaluate the neuroprotective effects of 2-BFI and new compounds **B06-red**, **BIN02**, **BIN05**. The first part of this study was to determine the beneficial effect of the selected compounds in the *C. elegans* through the thrashing assay. The sample size for the intervention was chosen following previous studies in our laboratory and using one of the available interactive tool (https://www.biomath.info/power/index.html). According to each drug assay, we used n = 120–150 or 50–70 as total for at least 3 replicates in *C. elegans*.

4.5.2. Worm strains, maintenance, and general methods

Strains used in this work and abbreviations are listed in the Table 7. All the strains were backcrossed to Bristol strain N2 (WT) five to twelve times. Standard methods were used for culturing and observing *C. elegans*, unless otherwise noted. Wild-type nematodes were propagated at 20 °C, while transgenic strains were maintained at 16 °C in a temperature-controlled incubator on solid nematode growth medium (NGM) seeded with *Escherichia coli* (*E. coli*) OP50 strain as food source. To obtain the age synchronized population of eggs, gravid adults were treated with alkaline hypochlorite solution (0.5 M NaOH, ~2.6 % NaClO) for 5–7 min. Fertilized eggs were suspended in S-medium for 12 h and L1 larvae were allowed to hatch overnight in the absence of food.

4.5.3. Compounds preparation and treatment

The compounds were dissolved in 100 % DMSO. Each concentration was then dissolved in MilliQ purified water to achieve a final concentration of 10 μM in 1 % DMSO in well. For the thrashing assay, treatments were carried out in liquid culture for 4 days at 20 °C. Each well contained a final volume of 60 μL, consisting of 25–30 animals in the L1 stage, compounds under study at the appropriate doses, and OP50 inactivated by freeze–thaw cycles and incubated in S-medium complete to a final optical density of 595 (OD595) of 0.9–0.8 measured in the microplate reader.

Table 7
List of *C. elegans* strains used in this work.

Strain	Genotype	Source
CL2006	dvIs2 [pCL12(unc-54/human Abeta peptide 1–42 minigene) + rol-6(su1006)]	CGC

4.5.4. Thrashing assay

To assess the effect on locomotion through neurotransmitter imbalances, we employed the thrashing assay to quantify worm motility. For this, worms were placed in a liquid medium and the number of lateral swimming movements (thrashes sec^{-1}) was counted. A single thrash defined as a complete change in the direction of bending at the mid body (Fig. 9). Briefly, after chronic treatment in liquid culture, worms were transferred for 30 min to a fresh NGM plate. First, a small volume of M9 buffer was transferred to the glass slide. Next, 10 worms were randomly selected, allowed to stabilize in M9 buffer for 30 s, and each worm was analyzed separately or its motility over a 30-second period. Manual counting of thrashing was done. This assay was run per duplicate.

4.6. Statistical analysis

Figs. 6, 7 and 8 are expressed as the mean ± SD of triplicate determinations. Experiments were repeated at least three times, yielding similar results. Data were first analysed using one-way ANOVA. Then, a significance level of $p < 0.05$ was applied to the post hoc statistical analyses (Tukey test). The SPSS statistical software package (version 20.0) for Windows (Chicago, IL, USA) was used.

Declaration of Competing Interest

The authors declare that they have no known competing financial interests or personal relationships that could have appeared to influence the work reported in this paper.

Acknowledgments

This work was supported by Ministerio de Ciencia, Innovación y Universidades, Agencia Estatal de Investigación (Spain, PID2019-107991RB-I00, PID2022-1380790B-I00), Basque Government (IT-1211-19 and 1512-22), Generalitat de Catalunya (GC) (2021 SGR 00357) and PDC2022-133441-I00 (MCIN/AEI/ 10.13039/ 501100011033 and by the "European Union NextGenerationEU/PRTR) and by UCM-Santander (PR44/21-29931 to J.A.M.-G.). The project leading to these results has received funding from "la Caixa" Foundation (ID 100010434) under agreement CI18-00002. This activity has received funding from the European Institute of Innovation and Technology (EIT). This body of the European Union receives support from the European Union's Horizon 2020 research and innovation programme.

Appendix A. Supplementary data

Supplementary data to this article can be found online at https://doi.org/10.1016/j.bioorg.2023.106935.

References

[1] P. Bousquet, J. Feldman, J. Schwartz, Central cardiovascular effects of alpha adrenergic drugs: differences between catecholamines and imidazolines, J. Pharmacol. Exp. Ther. 230 (1984) 232–236.
[2] D.A. Ruggiero, S. Regunathan, H. Wang, T.A. Milner, D.J. Reis, Immunocytochemical localization of an imidazoline receptor protein in the central nervous system, Brain Res. 780 (1998) 270–293.
[3] J.A. Lowry, J.T. Brown, Significance of the imidazoline receptors in toxicology, Clin. Toxicol. 52 (2014) 454–469.
[4] J.X. Li, Imidazoline I_2 receptors: an update, Pharmacol. Ther. 178 (2017) 48–56.
[5] P. Bousquet, A. Hudson, J.A. García-Sevilla, J.X. Li, Imidazoline receptor system: the past, the present, and the future, Pharmacol. Rev. 72 (2020) 50–79.
[6] J.X. Li, Y. Zhang, Imidazoline I_2 receptors: target for new analgesics? Eur. J. Pharmacol. 658 (2011) 49–56.
[7] S. Regunathan, D.L. Feinstein, D.J. Reis, Anti-proliferative and anti-inflammatory actions of imidazoline agents. Are imidazoline receptors involved? Ann. N. Y. Acad. Sci. 881 (1999) 410–419.
[8] K.L. Smith, D.S. Jessop, D.P. Finn, Modulation of stress by imidazoline binding sites: implications for psychiatric disorders, Stress 12 (2009) 97–114.
[9] L.F. Callado, J.I. Martín-Gómez, J. Ruiz, J.M. Garibi, J.J. Meana, Imidazoline I_2 receptors density increases with the malignancy of human gliomas, J. Neurol. Neurosurg. Psychiatry 75 (2004) 785–787.
[10] J.J. Meana, F. Barturen, I. Martín, J.A. García-Sevilla, Evidence of increased non-adrenoreceptor [3H]idazoxan binding sites in the frontal cortex of depressed suicide victim, Biol. Psychiatry 34 (1993) 498–501.
[11] J. Ruíz, I. Martín, L.F. Callado, J.J. Meana, F. Barturen, J.A. García-Sevilla, Non-adrenoreceptor [3H]idazoxan binding sites (I2-imidazoline sites) are increased in postmortem brain from patients with Alzheimer's disease, Neurosci. Lett. 160 (1993) 109–112.
[12] C. Gargalidis-Moudanos, N. Pizzinat, F. Javoy-Agid, A. Remaury, A. Parini, I_2-imidazoline binding sites and monoamine oxidase activity in human postmortem brain from patients with Parkinson's disease, Neurochem. Int. 30 (1997) 31–36.
[13] H. Wilson, G. Dervenoulas, G. Pagano, R.J. Tyacke, S. Polychronis, J. Myers, R. N. Gunn, E.A. Rabiner, D. Nutt, M. Politis, Imidazoline 2 binding sites reflecting astroglia pathology in Parkinson's disease: an *in vivo* ^{11}C-BU99008 PET study, Brain 10 (2019) 3116–3128.
[14] C. Dardonville, I. Rozas, Imidazoline binding sites and their ligands: an overview of the different chemical structures, Med. Res. Rev. 24 (2004) 639–661.
[15] L.C. Rovati, N. Brambilla, T. Blicharski, J. Connell, C. Vitalini, A. Bonazzi, G. Giacovelli, F. Girolami, M. D'Amato, Efficacy and safety of the firts-in-class imidazoline-2 receptor ligand CR4056 in pain from knee osteoarthritis and disease phenotypes: a randomized, double-blind, placebo-controlled phase 2 trial, Osteoarthr. Cartil. 28 (2020) 22–30.
[16] R.J. Tyacke, J.F.M. Myers, A.V. Venkataraman, I. Mick, S. Turton, J. Passchier, S. M. Husband, E.A. Rabiner, R.N. Gunn, P.S. Murphy, C.A. Parker, D.J. Nutt, Evaluation of ^{11}C-BU99008, a PET ligand for the imidazoline2 binding site in human brain, J. Nucl. Med. 59 (2018) 1597–1602.
[17] S. Abás, A.M. Erdozain, B. Keller, S. Rodríguez-Arévalo, L.F. Callado, J.A. García-Sevilla, C. Escolano, Neuroprotective effects of a structurally new family of high affinity imidazoline I_2 receptors ligands, ACS Chem. Nerosci. 8 (2017) 737–742.
[18] S. Abás, C. Estarellas, F.J. Luque, C. Escolano, Easy acess to (2-imidazolin-4-yl) phosphonats by a micorowave assisted multicomponent reaction, Tetrahedron 71 (2015) 2872–2881.
[19] P. Nadal Rodríguez, O. Ghashghaei, A. Bagán, C. Escolano, R. Lavilla, Heterocycle-Based Multicomponent Reactions in Drug Discovery: From Hit Finding to Rational Design, Biomedicines 10 (2022) 1488.
[20] C. Griñán-Ferré, F. Vasilopoulou, S. Abás, S. Rodríguez-Arévalo, A. Bagán, F. X. Sureda, B. Pérez, L.F. Callado, J.A. García-Sevilla, M.J. García-Fuster, C. Escolano, M. Pallàs, Behavioral and cognitive improvement induced by novel imidazoline I_2 receptor ligands in female SAMP8 mice, Neurotherapeutics 16 (2019) 416–431.
[21] F. Vasilopoulou, A. Bagan, S. Rodríguez-Arévalo, C. Escolano, C. Griñán-Ferré, M. Pallàs, Amelioration of BPSD-like phenotype and cognitive decline in SAMP8 mice model accompanied by molecular changes after treatment with I1-imidazoline receptor ligand MCR5, Pharmaceutics 12 (2020) 475.
[22] F. Jiménez-Altayó, A. Cabrera, A. Bagán, L. Giménez-Llort, P. D'Ocon, B. Pérez, M. Pallàs, C. Escolano, An imidazoline 2 receptor ligand relaxes mouse aorta via off-target mechanisms resistant to aging, Front. Pharmacol. 13 (2022), 826837.
[23] F. Vasilopolou, S. Rodríguez-Arévalo, A. Bagán, C. Escolano, C. Griñán-Ferré, M. Pallàs, Disease-modifying treatment with I_2 imidazoline receptor ligand LSL60101 in an Alzheimer's disease mouse model: a comparative study with donepezil, Br. J. Pharmacol. 1–17 (2021).
[24] S. Rodriguez-Arévalo, A. Bagán, C. Griñán-Ferré, F. Vasilopoulou, M. Pallàs, I. Brocos-Mosquera, L.F. Callado, M.I. Loza, A.L. Martínez, J. Brea, B. Pérez, E. Molins, S. De Jonghe, D. Daelemans, M. Radan, T. Dijikic, K. Nikolic, E. Hernández-Hernández, M.J. García-Fuster, J.A. García-Sevilla, C. Escolano, Benzofuranyl-2-imidazoles as Imidazoline I_2 Receptor Ligands for Alzheimer's Disease, Eur. J. Med. Chem.. 222 (2021), 113540.
[25] C. Escolano, M. Pallás, C. Griñán-Ferré, S. Abás, L.-F. Callado, J. A. García-Sevilla, Synthetic I_2 Imidazoline Receptor Ligands for Prevention or Treatment of Human Brain Disorders. WO 2019/121853 A1, June 27, 2019.
[26] F. Vasilopoulou, C. Griñán-Ferré, S. Rodríguez-Arévalo, A. Bagán, S. Abás, C. Escolano, M. Pallàs, I_2 imidazoline receptor modulation protects aged SAMP8 mice against cognitive decline by suppressing the calcineurin pathway, GeroScience 43 (2020) 965–983.
[27] S. Abás, S. Rodríguez-Arévalo, A. Bagán, C. Griñán-Ferré, F. Vasilopoulou, I. Brocos-Mosquera, C. Muguruza, B. Pérez, E. Molins, F.J. Luque, P. Pérez-Lozano, S. de Jonghe, D. Daelemans, L. Naesens, J. Brea, M.I. Loza, E. Hernández-Hernández, J.A. García-Sevilla, M.J. García-Fuster, M. Radan, T. Djikic, K. Nikolic, M. Pallàs, L.F. Callado, C. Escolano, Bicyclic α-Iminophosphonates as High Affinity Imidazoline I_2 Receptor Ligands for Alzheimer's Disease, J. Med. Chem.. 7 (2020) 3610–3633.
[28] A. Bagán, J.A. Morales-García, C. Griñán-Ferré, C. Díaz, J.P. Palacio, M.C. Ramos, F. Vicente, B. Pérez, J. Brea, M.I. Loza, M. Pallàs, C. Escolano, Insights into the pharmacokinetics and in vitro cell-based studies of the imidazoline I_2 receptor ligand B06, Int. J. Mol. Sci. 23 (2022) 5408.
[29] V.P. Kukhar, H.P. Hudson (Eds.), Aminophosphonic and Aminophosphinic Acids, Chemistry and Biological Activity; Wiley, New York, NY, USA, 1999.
[30] K. Moonen, I. Laureyn, C.V. Stevens, Synthetic methods for azaheterocyclic phosphonates and their biological activity, Chem. Rev. 104 (2004) 6177–6215.
[31] E.D. Naydenova, P.T. Todoro, Kolio D. Troev, Recent Synthesis of Aminophosphonic Acids as Potential Biological Importance, Amino Acids 38 (2010) 23–30.
[32] A. Mucha, P. Kafarski, L. Berlicki, Remarkable Potential of the α-Aminophosphonate/Phosphinate Structural Motif in Medicinal Chemistry, J Med. Chem. 54 (2011) 5955–5980.

[33] M. Ordoñez, J.L. Viveros-Ceballosa, C. Cativiela, F.J. Sayago, An update on the stereoselective synthesis of α-aminophosphonic acids and derivatives, Tetrahedron 71 (2015) 1745–1784.
[34] I.E. Głowacka, A. Hartwich, I. Rozpara, D.G. Piotrowska, Synthesis of Functionalized Diethyl(pyrrolidin-2-yl)phosphonate and Diethyl(5-oxopyrrolidin-2-yl)phosphonate, Molecules 26 (2021) 3160.
[35] E.I. Martínez-Toto, M. Ordóñez, J.C. Morales-Solís, M. Flores-Alamo, Diastereoselective Phosphonylation of Chiral Cyclic Imines for the Synthesis of Phosphoproline Derivatives, Eur. J. Org. Chem. (2022) e202200461.
[36] A.S. Gazizov, A.V. Smolobochkin, R.A. Turmanov, M.A. Pudovik, A.R. Burilova, O. G. Sinyashin, Synthesis of Phosphaproline Derivatives: A Short Overview, Synthesis 51 (2019) 3397–3409.
[37] C. Griñán-Ferré, A. Bellver-Sanchis, M. Olivares-Martín, O. Bañuelos-Hortigüela, M. Pallàs, Synergistic Neuroprotective Effects of a Natural Product Mixture against AD Hallmarks and Cognitive Decline in Caenorhabditis elegans and an SAMP8 Mice Model, Nutrients 13 (2021) 2411.
[38] H. Xi, T. Tao, R. Zhang, X. Xue, Y. Zhu, J. Liu, X. Xin, X. Zeng, The 2-(2-benzofuranyl)-2-imidazoline provides neuroprotection against focal cerebral ischemia-reperfusion injury in diabetic rats: Influence of microglia and possible mechanisms of action, Brain Res. Bull. 174 (2021) 230–239.
[39] J. Tian, R. Chen, L. Hu, L. Zhang, J. Chen, Y. Cao, X. Guo, L. Wang, Z. Han, The protective effect of 2-(2-benzonfuranyl)- 2-imidazoline against oxygen-glucose deprivation in cultured rat cortical astrocytes, Neurosci. Res. 133 (2018) 1–6.
[40] J.S. Tian, Q.J. Zhai, Y. Zhao, R. Chen, L.D. Zhao, 2-(2-benzofuranyl)-2-imidazoline (2-BFI) improved the impairments in AD rat models by inhibiting oxidative stress, inflammation, and apoptosis, J. Integr. Neurosci. 16 (2017) 385–400.
[41] C. Arróniz, J. Molina, S. Abás, E. Molins, J.M. Campanera, F.J. Luque, C. Escolano, First diastereoselective [3+2] cycloaddition reaction of diethyl isocyanomethylphosphonate and maleimides, Org. Biomol. Chem. 11 (2013) 1640–1649.
[42] S. Padilla, J. Adrio, J.C. Carretero, Au-Catalyzed Asymmetric Formal [3 + 2] Cycloaddition of Isocyanoacetates with Maleimides, J. Org. Chem. 77 (2012) 4161–4166.
[43] For a unique example of analogous structure see: H. A. Dondas, Y. Durust, R. Grigg, M. J. Slatera, M. A. B. Sarker, X=Y=ZH systems as potential 1,3-dipoles. Part 62: 1,3-Dipolar cycloaddition reactions of metallo-azomethine ylides derived from α-iminophosphonates, Tetrahedron 61 (2005) 10667–10682.
[44] A. Massarotti, F. Brunelli, S. Aprile, M. Giustiniano, G.C. Tron, Medicinal Chemistry of Isocyanides, Chem. Rev. 121 (2021) 10742–10788.
[45] K. Kawashima, A. Kakehib, M. Noguchi, Generation of functionalized azomethine ylides and their application to stereoselective heterocycle synthesis: an equivalent process of C-unsubstituted nitrile ylide cycloaddition reaction, Tetrahedron 63 (2007) 1630–1643.
[46] P. Erti, Calculation of molecular properties and bioactivity score. http://www.molinspiration.com/.
[47] A. Daina, O. Michielin, V. Zoete, SwissADME: a free web tool to evaluate pharmacokinetics, drug-likeness and medicinal chemistry friendliness of small molecules, Sci. Rep. 7 (2017) 42717.
[48] B. Grijalba, L.F. Callado, J.J. Meana, J.A. García-Sevilla, A. Pazos, α2-Adrenoceptor subtypes in the human brain: a pharmacological delineation of [3H]RX-821002 binding to membranes and tissue sections, Eur. J. Pharmacol. 310 (1996) 83–93.
[49] L.F. Callado, A.I. Maeztu, J. Ballesteros, M. Gutiérrez, J.J. Meana, Differential [3H] idazoxan and [3H]2-(2-benzofuranyl)-2- imidazoline (2-BFI) binding to imidazoline I2 receptors in human postmortem frontal cortex, Eur. J. Pharmacol. 423 (2001) 109–114.
[50] L. Di, E.H. Kerns, K. Fan, O.J. McConnelll, G.T. Carter, High throughput artificial membrane permeability assay for blood-brain barrier, Eur. J. Chem. 38 (2003) 223–232.
[51] M. Fukui, J.-H. Song, J. Choi, H.J. Choi, B.T. Zhu, Mechanism of glutamate-induced neurotoxicity in HT22 mouse hippocampal cells, Eur. J. Pharmacol. 617 (2009) 1–11.
[52] A. Krishna, M. Biryukov, C. Trefois, P.M.A. Antony, R. Hussong, J. Lin, M. Heinäniemi, G. Glusman, S. Köglsberger, O. Boyd, B.H.J. Berg, D. Linke, D. Huang, K. Wang, L. Hood, A. Tholey, R. Schneider, D.J. Galas, R. Balling, P. May, Systems genòmics evaluation of theSH-SY5Y neuroblastoma cell line as a model for Parkinson's disease, BMC Genom. 15 (2014) 1154.
[53] S. Regunathan, D.J. Reis, Imidazoline receptors and their endogenous ligands, Annu. Rev. Pharmacol. Toxicol. 36 (1996) 511–544.
[54] G.M. Sheldrick, Crystal structure refinement with SHELXL, Acta Cryst. C71 (2015) 3–8.
[55] L.J. Farrugia, WinGXandORTEP for Windows: an update, J. Appl. Cryst. 45 (2012) 849–854.
[56] J.A. Morales-Garcia, S. Alonso-Gil, A. Santos, A. Perez-Castillo, Phosphodiesterase 7 Regulation in Cellular and Rodent Models of Parkinson's Disease, Mol. Biol. 57 (2020) 806–822.